THE INFLUENCE OF SHEARWISE VERTICAL MOTIONS ON THE DEVELOPMENT OF AN INTENSE UPPER-LEVEL FRONT

by

ANDREA A. LANG and JONATHAN E. MARTIN

Department of Atmospheric and Oceanic Sciences
University of Wisconsin-Madison
1225 W. Dayton Street
Madison, WI 53706
Ph. (608) 262-9845
Fax (608) 262-0166
jemarti1@wisc.edu

Submitted for publication to *Monthly Weather Review*: August 22, 2007
Revised version submitted: May 2, 2008

ABSTRACT

The total quasi-geostrophic (QG) vertical motion is partitioned into transverse and shearwise couplets oriented parallel to, and along, the geostrophic vertical shear, respectively, in order to examine the role of rotational frontogenesis, and its associated shearwise circulation, in the life cycle of an upper-front/jet system in northwesterly flow. The analysis reveals that shearwise subsidence is a persistent and significant mode of frontogenetical subsidence throughout the life cycle. Given the physical relationship between shearwise vertical motions and rotational frontogenesis, it is suggested that the contributions of rotational frontogenesis to the life cycle of an upper-front/jet are twofold.

First, positive rotational frontogenesis, characterized by along-shear **Q**-vectors, provides forcing for cyclonic rotation of $\nabla\theta$ near the base of the geopotential height trough (or, more generally, in the vicinity of the vorticity maximum) thereby sustaining the positive rotational frontogenesis first initiated by along-shear tilting upstream of the vorticity maximum. The associated cyclonic rotation of $\nabla\theta$ promotes the development of cold air advection along the jet axis leading to the establishment of a transverse vertical circulation with subsidence on or to the warm side of the baroclinic zone that provides positive scalar frontogenetic tilting, the well known Shapiro effect. Second, the important rotational frontogenesis is itself directly associated with a secondary vertical circulation, the shearwise circulation, that also contributes to scalar frontogenetic tilting just upshear of a developing thermal trough. Though the transverse subsidence becomes larger later in the upper-front life cycle, it is accompanied by an equally large, or larger, contribution to frontogenetic tilting delivered by the shearwise subsidence associated with continued rotational frontogenesis. The superposition of the transverse and shearwise subsidence maxima, associated with the

Shapiro effect and the rotational frontogenesis that enhances the Shapiro effect, respectively, leads to a period of rapid frontogenesis.

1. Introduction

A distinguishing feature of the baroclinic wave life cycle is the development of narrow zones of enhanced temperature and momentum gradients known as frontal zones. Such zones are characterized by large density contrasts, enhanced static stability, local maxima in vertical vorticity, strong vertical wind shear, widths of order 100 km, and lengths of order 1000 km. Though baroclinic zones with these frontal properties can exist throughout the entire depth of the troposphere and lower stratosphere, they are particularly robust near the Earth's surface (surface fronts) where an impermeable solid boundary exists and at upper-levels (upper-level fronts) near the *thermodynamic* boundary represented by the tropopause.

In an early investigation of what would later be termed upper-level fronts, Palmen and Nagler (1949) concluded that these baroclinic zones were not intensified through differential horizontal advection as is the case with their surface counterparts. Instead, they suggested that descent (ascent) upstream (downstream) of an upper tropospheric trough axis superimposed upon a cross-stream vertical circulation combined to strongly influence the development of such upper baroclinic zones.

The pioneering work of Reed and Sanders (1953) and Reed (1955) suggested that upper-level fronts and their associated folded tropopause structures were ubiquitous features of the mid-latitude atmosphere. Reed and Sanders (1953) noted that differential subsidence was responsible for intensifying the horizontal temperature gradient associated with such

features and described it as being distributed in couplets straddling the front itself. Thus, they claimed that the primary physical driver of upper-level frontogenesis was isentropic tilting associated with differential, across-front vertical motion.

A comprehensive review of the first 50 years of research concerning the structure and dynamics of these upper-level fronts is provided by Keyser and Shapiro (1986). From among the many topics discussed and questions raised therein, the nature of the vertical motions involved in upper-level frontogenesis, and the environments within which these vertical motions develop, are most germane to the present study. The Sawyer (1956)-Eliassen (1962) equation was the first diagnostic tool to explicitly make the connection between frontogenetic forcing (stretching and shearing deformation in geostrophic flow) and the production of the transverse ageostrophic circulation. Arguing from the Sawyer-Eliassen perspective, Shapiro (1981) suggested that the subsiding branch of the direct circulation in the jet entrance region could strengthen and shift toward the warm side of an upper baroclinic zone when cold air advection occurred along the jet (i.e. what was later termed the Shapiro effect by Rotunno et al. (1994)). This suggestion was demonstrated in a 2D, primitive equation simulation by Keyser and Pecnick (1985) who found subsidence maximized beneath the jet core under such circumstances. Such a distribution of vertical motion is strongly upper-frontogenetical.

The development of cold air advection along the maturing upper-level front, central to the initiation of the frontogenetical Shapiro effect, has been examined from both idealized modeling and observational perspectives. Rotunno et al. (1994) (hereafter RSS94) analyzed

normal mode cyclogenesis in a primitive equation (PE) channel model to examine the upper frontogenesis process in an atmosphere with a constant potential vorticity (PV) stratosphere. They considered the transition from a nearly equivalent barotropic environment, with little or no along-front thermal advection in the upper troposphere, to an environment characterized by strong cold air advection near the base of an upper trough just a day later. They argued that the development of cold air advection along the front was initiated by subsidence maximized slightly downstream of the northwesterly flow inflection between a ridge and downstream trough. This subsidence was shown to be a portion of a thermally direct vertical circulation associated with confluent frontogenesis. The along-flow increase in the strength of the subsidence induced a cyclonic rotation of the isentropes which reoriented the isentropes relative to the isohypses and promoted the development of cold air advection.

In their observational study, Schultz and Doswell (1999) (hereafter SD99) extended the 2D vector frontogenesis formulation of Keyser et al. (1988) to include the 3D terms related to vertical tilting in order to consider the mechanism(s) underlying the initiation and distribution of along-front cold air advection in an observed case of northwesterly flow upper-level frontogenesis[1]. Their rotational frontogenesis expression contained a tilting term in which along-isentrope gradients of ω are required in order for tilting to play a role in the rotation of $\nabla\theta$. Diagnostic evaluation of a case of northwesterly flow upper frontogenesis led SD99 to conclude that the aforementioned tilting term was of second order importance

[1] They also considered a case of the less studied southwesterly flow upper-level frontogenesis from this perspective and found that increasing cold air advection along the

compared to the influence of rotation associated with vertical vorticity. They were thus led to emphasize the role of horizontal winds in the rotation of isentropes in establishing cold air advection along the front[2] and suggested a primary role for rotational frontogenesis in the upper frontal life cycle. However, since their vector frontogenesis diagnostics were calculated using the full wind, it was not possible for SD99 to identify a discrete vertical circulation attributable to this important rotational frontogenesis.

As first pointed out by Keyser et al. (1988), and explored more thoroughly by Keyser et al. (1992), the $\boldsymbol{Q}$-vector (Hoskins et al. 1978) is the quasi-geostrophic (QG) version of the 2D vector frontogenesis function. They demonstrated that partitioning the $\boldsymbol{Q}$-vector into along and across isentrope components successfully described the forcing for two orthogonal components of the total QG vertical motion (ω) field. The across-isentrope component, which describes the rate of change of $|\nabla\theta|$ (i.e. scalar frontogenesis) is associated with elongated, often banded, couplets of vertical motion oriented parallel to the geostrophic vertical shear, the traditional transverse couplets (to be denoted as ω_n). The along-isentrope component, which describes the rate of change of the direction of $\nabla\theta$ (i.e. rotational frontogenesis) is associated with cellular dipoles of vertical motion aligned along the geostrophic vertical shear. Such couplets were referred to as shearwise couplets by Martin (2006) and will be denoted as ω_s. The present study utilizes this QG omega equation perspective to examine the contributions to upper-level frontogenesis made by the discrete

---

front was related to an upstream vorticity maximum in both cases.

[2] A similar conclusion with regard to this question, based upon examination of a thermal

vertical circulations attributed to the separate QG scalar and rotational frontogenesis throughout a portion of the life cycle of a robust upper-front. It will be shown that the shearwise subsidence is the predominant mode of frontogenetical subsidence throughout the life cycle. This predominance underscores the importance of the rotational frontogenesis process in the life cycle of upper level fronts and provides motivation for attempting to clarify the means by which scalar and rotational frontogenesis interact to both establish and maintain the kinematic and thermodynamic ingredients conducive to upper frontogenesis.

The paper is structured in the following manner. Section 2 provides a description of vector frontogenesis and its QG equivalent which leads directly to the method of partitioning QG omega. Section 3 provides a synoptic overview of the upper-front of interest. Analysis of the QG vertical motion associated with the evolution of this robust upper-front is presented in Section 4. Section 5 provides analysis and discussion of the results while Section 6 offers a summary and points to future work.

2. Vector frontogenesis and vertical motion

Petterssen (1936) was the first to suggest that frontogenesis might be quantified by considering

$$F = \frac{d}{dt}\left|\nabla\theta\right| \qquad (1)$$

the rate of change of the magnitude of the horizontal potential temperature gradient produced

---

advection tendency equation, was reached by Schultz and Sanders (2002).

through advection by the horizontal wind only ($\mathbf{V}_H = u\mathbf{i} + v\mathbf{j}$). Keyser et al. (1988) provided a generalization of the Petterssen frontogenesis equation, by examining the Lagrangian rate of change of the *magnitude* and *direction* of the horizontal potential temperature gradient vector,

$$\boldsymbol{F} = \frac{d}{dt}\nabla\theta. \qquad (2)$$

In their formulation, they considered the effect of the horizontal wind only, so that $\frac{d}{dt} = \frac{d}{dt} + u\frac{\partial}{\partial x} + v\frac{\partial}{\partial y}$. Keyser et al. (1988) exploited this conceptual extension of $\boldsymbol{F}$ by considering components using a natural coordinate system, defined by the local orientation of the isentropes in the horizontal plane such that $\hat{n}$ was directed across the isentropes toward colder air and $\hat{s}$ was 90° clockwise of $\hat{n}$. In such a coordinate frame, $\boldsymbol{F} = F_n\hat{n} + F_s\hat{s}$. Frontogenetic forcing in the $\hat{n}$ direction was referred to as *scalar* frontogenesis or F_n and is equal to

$$F_n = -\frac{|\nabla\theta|}{2}[E\cos 2\beta - D] \qquad (3)$$

where E is the total deformation, D is the divergence and β is the angle between the isentropes and the axis of dilatation of the total deformation field. This type of forcing was associated with a modification of the *magnitude* of the potential temperature gradient and was equivalent to Petterssen's frontogenesis equation (note that $F_n < 0$ describes frontogenesis). Frontogenetic forcing in the $\hat{s}$ direction was referred to as *rotational* frontogenesis or F_s and is equal to

$$F_s = \frac{|\nabla\theta|}{2}[E\sin 2\beta + \zeta] \qquad (4)$$

where ζ is the vertical vorticity. This type of forcing resulted in a modification of the *direction* of the potential temperature gradient vector.

Taking up the suggestion made by Keyser et al. (1988), who noted that the so-called $\boldsymbol{Q}$ vector, introduced by Hoskins et al. (1978), was the QG form of (2), Keyser et al. (1992) applied the quasi-geostrophic (QG) assumption to $\boldsymbol{F}$. Exploiting the fact that for horizontal adiabatic flow,

$$\boldsymbol{Q} = \frac{d}{dt}_g \nabla_p\theta \qquad (5)$$

where $\frac{d}{dt}_g = \frac{d}{dt} + u_g\frac{\partial}{\partial x} + v_g\frac{\partial}{\partial y}$ and p represents differentiation on a constant pressure surface, they employed a similar natural coordinate partitioning of $\boldsymbol{Q}$ where $\boldsymbol{Q} = Q_n\hat{n} + Q_s\hat{s}$. The across isentrope component of $\boldsymbol{Q}$ ($\boldsymbol{Q_n} = Q_n\hat{n}$) describes the rate of change of the *magnitude* of $\nabla\theta$ following the geostrophic wind and has a magnitude given by,

$$Q_n = -\frac{\boldsymbol{Q}\cdot\nabla\theta}{|\nabla\theta|} \text{ with } \hat{n} = -\frac{\nabla\theta}{|\nabla\theta|}. \qquad (6)$$

The along isentrope component of $\boldsymbol{Q}$ ($\boldsymbol{Q_s} = Q_s\hat{s}$) describes the rate of change of the *direction* of $\nabla\theta$ following the geostrophic wind and has a magnitude given by

$$Q_s = \frac{\boldsymbol{Q}\cdot(\hat{k}\times\nabla\theta)}{|\nabla\theta|} \text{ with } \hat{s} = \frac{\hat{k}\times\nabla\theta}{|\nabla\theta|}. \qquad (7)$$

Since the QG omega equation

$$\sigma(\nabla^2 + \frac{f_o^{\,2}}{\sigma}\frac{\partial^2}{\partial p^2})\omega = -2\nabla\cdot\boldsymbol{Q} \qquad (8)$$

describes the vertical motion (ω) forced by the divergence of the QG equivalent of ***F***, the ***Q*** vector, using the partitioned ***Q*** vector allows the separate QG omega fields associated with rotational and scalar QG vector frontogenesis to be isolated. Motivated by a desire to develop a more comprehensive understanding of the role of rotational frontogenesis in the development of upper-level frontal zones, here we employ the QG frontogenesis perspective, rooted in the components of the partitioned ***Q*** vector, in order to explicitly examine the distribution of both the shearwise (ω_s) and transverse (ω_n) vertical motions throughout the life-cycle of a robust upper-level front. The analysis begins with a synoptic overview of the upper-level front in question.

3. Synoptic Overview

During the second week of November 2003, a high amplitude flow developed over North America with the polar jet dipping southward from 60°N to roughly 40°N along the west coast of North America, while the sub-tropical jet sliced northeastward from well off the coast of southern California to Michigan. The northwesterly flow along the west coast was characterized by a region of strong baroclinicity that subsequently evolved into a potent upper-front.

At 1200 UTC 11 November, a high amplitude flow pattern over North America was evident as a strongly baroclinic northwesterly flow entered the northwest United States (Fig. 1a). At 400 hPa this baroclinic zone contained a strip of vorticity oriented along the isentropes from extreme southeastern Alaska to Washington. Downstream of the Pacific

Northwest, the baroclinic zone weakened. Another noteworthy feature was the dominant positively tilted shortwave trough that stretched southwestward from southwestern Wyoming across the California coast into the Pacific Ocean. The upper-level flow over the United States was characterized by a second baroclinic zone that originated downstream of the axis of this shortwave and stretched northeastward over the Rockies to Great Lakes region (Fig. 1a). The jet associated with this shortwave possessed winds exceeding 70 m s^{-1} over the central Plains (Fig. 1b). At this time, the polar jet was oriented nearly perpendicularly to the sub-tropical jet, and was also a fairly linear feature with a maximum speed of 70 m s^{-1} over southeast Alaska (Fig. 1b).

By 0000 UTC 12 November, the northern 400 hPa shortwave, located at the left exit region of the polar jet, had shifted slightly eastward as had its associated baroclinic zone (Fig. 2a). The southern extremity of this developing upper-front reached further south than at the previous time, extending into southwestern Wyoming. The amplification of the 400 hPa thermal trough was also significant by this time, with its axis stretching from central Alberta, through central Montana, into Wyoming. At 300 hPa the northwesterly jet axis was also oriented more or less along the isentropes that defined the upper-front. The maximum wind speed, centered over the British Columbia-Alberta border, had decreased to just over 60 m s^{-1} (Fig. 2b). This jet exhibited an abrupt exit region, situated near the Idaho-Wyoming border, where the flow joined the northwestern edge of the southwesterly sub-tropical jet along the front range of the Rocky Mountains.

At 1200 UTC 12 November the intensity of the upper-level front increased from

Alberta southward into the northern Plains of the United States where it reached the base of the geopotential height trough over northcentral Nebraska. The strongest portion of the front was centered on the eastern border of Wyoming, where the potential temperature gradient was ~5.25 K (100 km)$^{-1}$ (Fig. 3a). At 300 hPa, the abrupt exit region of the northwesterly jet weakened. The flow joined the southwesterly jet streak, creating a meandering polar jet which had several speed maxima of over 60 m s^{-1} scattered across northern Alberta, the central Plains, and the southern Great Lakes regions (Fig. 3b).

The upper-front continued its progression though the base of the shortwave trough over the central Plains so that by 1800 UTC 12 November the absolute vorticity maximum and the most intense segment of the upper-front were located within the base of this trough and stretched from eastern Montana through South Dakota and eastward into southern Wisconsin (Fig. 4a). Though the 300 hPa northerly jet centered over northwestern Saskatchewan was sustained at 60 m s^{-1} (Fig. 4b), the jet maximum situated over the Plains had become the dominant jet feature. It had intensified to over 70 m s^{-1}, was located over central Iowa, and was characterized by weak geostrophic cold air advection as implied by the orientation of the isohypses and isentropes in Fig. 4a.

By 0000 UTC 13 November the intense upper-front stretched from the northern Plains to the Great Lakes region where the front emerged in the southwesterly flow over lower Michigan (Fig. 5a). The magnitude of the potential temperature gradient was also the strongest at this time, with a magnitude of ~ 8 K (100 km)$^{-1}$ along the eastern border of Iowa. The absolute vorticity at 400 hPa was oriented in a strip along the upper-front, with a local

maximum at the eastern edge of the frontal zone (Fig. 5a). The 300 hPa jet streak centered over southern Iowa continued to intensify, reaching speeds of over 80 m s^{-1} by this time (Fig. 5b). The jet axis was oriented along the warm side of the upper-front with increased geostrophic cold air advection through the jet core, implied, as before, in Fig. 5a. After this time, the upper-front became a component of a troposphere-deep frontal structure associated with the cyclogenesis event described by Martin (2006).

4. Quasi-Geostrophic Vertical Motion

In this section, gridded model analyses from the National Centers for Environmental Prediction's (NCEP's) Eta model (Eta 104-grid) are used in the calculation of QG omega and its components. These gridded data are first bilinearly interpolated from their original output grid to a 1°x1° latitude–longitude grid at 19 isobaric levels (from 1000 to 100 hPa at 50 hPa intervals) using an interpolation program included in the General Meteorological Analysis Package (GEMPAK). The gridpoint height and temperature data are then subjected to a Gaussian smoother that eliminates roughly 2/3 of the energy at wavelengths ≤ 660 km, equivalent to the cowbell filter described by Barnes et al. (1996) for use in quasi-geostrophic diagnostics with meso-scale models. Employing the technique of successive over relaxation (SOR), we then solve the *f*-plane version of the QG omega equation using a spatially averaged static stability that varies for each time with f_o set equal to the central latitude (45.5°N) of the domain for this case. With geostrophic forcing corresponding to the

divergences of $\boldsymbol{Q}$, $\boldsymbol{Q}_n$, and $\boldsymbol{Q}_s$, the total, transverse, and shearwise QG vertical motions, respectively, are returned in units of Pa s^{-1}. The subsequent analysis centers on the evolution of QG omega at both the 400 hPa level and in vertical cross sections corresponding to the time periods analyzed in Section 3.

The 400 hPa total QG vertical motion field along with the tilting scalar frontogenesis (hereafter *tilting frontogenesis*) at 1200 UTC 11 November is shown in Fig. 6a. The northwesterly flow baroclinic zone was characterized by several pockets of subsidence along the Canadian west coast (Fig. 6a) that combined to produce a nearly continuous swath of positive tilting frontogenesis on the cyclonic shear side of the upper baroclinic zone throughout British Columbia. At the southern end of the baroclinic zone, ascent was located from eastern Washington to southern Alberta and the isentropes became diffluent immediately downstream of this region. In the partitioned omega fields, pockets of shearwise omega captured nearly all of the full QG vertical motion in the northwesterly flow (Fig. 6b) and were associated with local regions of tilting frontogenesis along the front. Meanwhile, the transverse omega contributed very little to the full QG omega in the vicinity of the upper-front (Fig. 6c) and correspondingly meager tilting frontogenesis. The relatively strong couplet of shearwise omega located over southern British Columbia and Washington state (Fig. 6b) was related to $\boldsymbol{Q}_s$ vectors that were associated with positive rotational frontogenesis and a corresponding counterclockwise rotation of the isentropes along that portion of the baroclinic zone.

Several cross-sections perpendicular to the upper-front at this time (along the line A-

A' in Fig. 6a) were constructed. The total QG omega along this line, illustrated in Fig. 7a, shows subsidence between 325 hPa and 800 hPa, with a maximum centered at approximately 475 hPa, slightly on the warm side the baroclinic zone beneath the jet core. This distribution contributed to intensification of the upper-front via frontogenetic tilting from the tropopause to ~600 hPa on the cyclonic shear side of the jet. Nearly all of the differential subsidence across the baroclinic zone, and the resulting frontogenesis, was accounted for by the shearwise component of vertical motion (Fig. 7b), as the transverse vertical motion contributed very little (Fig. 7c).

At 0000 UTC 12 November, subsidence continued to dominate the total QG vertical motion in the northwesterly flow as the upper-front intensified (Fig 8a). The southern portion of the frontal zone, located from the Montana/Alberta border to central Wyoming, was characterized by the largest subsidence with three local maxima on the warm side of the front contributing to dramatically larger tilting frontogenesis than had been seen earlier. The $\boldsymbol{Q}_s$ vectors along this portion of the frontal zone were associated with continued positive rotational frontogenesis (Fig. 8b). The corresponding shearwise omega field (Fig. 8b), though contributing the largest share of the total descent, was not dominant, as was the case at the previous time, as the transverse component of QG omega played a larger role in forcing warm side subsidence along this portion of the front by this time (Fig. 8c). In fact, the linear nature of the total tilting frontogenesis there was a result of the geometry of the transverse contribution, though the magnitude of the total frontogenesis was shared equally between the shearwise and transverse vertical motions at this time.

Several vertical cross-sections perpendicular to the upper-front at this time (along line B-B' in Fig. 8a) are shown in Fig. 9. These sections cut through the northern region of maximum subsidence within the upper frontal zone. QG subsidence characterized the entire depth of the troposphere beneath the jet core, with a local maximum between 600 to 300 hPa within the upper-front (Fig. 9a). The resulting tilting frontogenesis was strong between the tropopause and ~550 hPa on the cyclonic shear side of the jet core. Shearwise omega was responsible for the majority of the subsidence, and roughly half of the tilting frontogenesis, throughout the depth of the troposphere (Fig. 9b). The small patch of transverse subsidence located on the warm side of the upper-front, with a maximum centered at approximately 400 hPa, was in a position where it too contributed to the thermally indirect circulation that promoted upper frontogenesis on the cyclonic shear side of the jet (Fig. 9c).

The distribution of vertical motion at 1200 UTC 12 November was characterized by an amplified region of subsidence on the warm edge of the frontal zone on the Montana/Wyoming border (Fig. 10a) This subsidence, with a magnitude of approximately 12 dPa s^{-1}, and a region of weak ascent downstream of the upper-front, formed a couplet that straddled the base of thermal trough in the northern Plains. Associated with this strong subsidence was extremely strong tilting frontogenesis (more than twice as large as at 0000 UTC 12 November) along an axis from southeastern Montana to northeastern Nebraska. The $\boldsymbol{Q_s}$ vectors were large in the base of the thermal trough, illustrating the substantial positive rotational frontogenesis that continued along the southern extent of the frontal zone. The corresponding shearwise omega was largely responsible for the couplet and continued to

contribute the majority of vertical motion associated with the developing upper-front (Fig. 10b). However, the contribution by the transverse omega continued to increase, with a band of subsidence oriented along and to the warm side of the most intense portion of the upper-front from southeastern Montana to southeastern Nebraska (Fig. 10c) which contributed to strong tilting frontogenesis from southeastern Montana through South Dakota. The shearwise omega contribution to tilting frontogenesis was nearly coincident, of comparable magnitude nearly everywhere and of greater magnitude in southeastern Montana (Fig. 10b).

Vertical cross sections just upstream of the thermal trough at this time are shown in Fig. 11. The subsidence maximum toward the warm side of the frontal zone was responsible for significant tilting frontogenesis on the cyclonic shear side of the jet from the tropopause to ~600 hPa (Fig. 11a). Roughly 60% of the tilting frontogenesis was associated with the shearwise subsidence (Fig. 11b) with the remainder contributed by the weaker transverse subsidence (Fig. 11c).

By 1800 UTC 12 November there was a noticeable change in the QG omega field (Fig. 12a). The strongest subsidence had moved into the base of the thermal trough along the South Dakota/Nebraska border and intensified significantly, to approximately 15 dPa s^{-1}. Downstream of the most intense portion of the upper-front, over Minnesota and Wisconsin, the pocket of ascent also intensified to approximately 7 dPa s^{-1}. This distribution of vertical motion was associated with quadrapole of tilting frontogenesis with a large maxima in South Dakota and a lesser maxima over Iowa and southern Wisconsin. Shearwise omega continued to account for nearly all of the vertical motion both upstream and downstream of the thermal

trough within the northwesterly flow (Fig. 12b). Within the upper-front, which had reached the base of the thermal trough, shearwise omega over Nebraska and South Dakota, contributed approximately 11 dPa s^{-1} of subsidence and was associated with the tilting frontogenesis maximum in South Dakota. Meanwhile, the transverse omega field, with a modest (~ 5 dPa s^{-1}) subsidence maxima on the South Dakota/Nebraska border, contributed to substantial tilting frontogenesis from western North Dakota toward Lake Michigan. Rotational frontogenesis remained large and positive along the base of the thermal trough as evidenced by the orientation and magnitude of the $\boldsymbol{Q_s}$ vectors (Fig. 12b).

Several cross-sections through the maximum subsidence along the Nebraska/South Dakota border at this time (along line D-D' in Fig. 12a) are shown in Fig. 13. The total QG subsidence maximum was approximately 15 dPa s^{-1} at 450 hPa, extended through the entire depth of the troposphere and was associated with a robust tilting frontogenesis maximum on the cyclonic shear side of the jet from the tropopause to ~600 hPa (Fig. 13a). Shearwise omega contributed roughly 2/3 of the magnitude of subsidence, with a 10 dPa s^{-1} maximum centered near 500 hPa within the upper-front (Fig. 13b). Correspondingly, more than 60% of the tilting frontogenesis was associated with the shearwise subsidence. By this time, the thermally direct circulation in the entrance region of the jet streak was apparent in the transverse omega field. The center of this circulation was shifted toward the warm side of the upper-front as is the case in regions of cold air advection along the jet axis (Keyser and Pecnick, 1985). The increasing importance of transverse omega to upper frontogenesis is manifested in the significant subsidence (roughly 5 dPa s^{-1}) centered at 500 hPa (Fig. 13c).

The transverse subsidence in the upper troposphere was positioned in such a way that it aided the upper frontogenesis over the Plains, though that contribution was limited in vertical extent, being largely contained above 550 hPa (Fig. 13c).

By 0000 UTC 13 November the magnitude of QG ascent downstream of the upper-front surpassed the magnitude of QG subsidence within the upper-front (Fig. 14a) which had weakened substantially in the six hour period, to approximately 10 dPa s^{-1}. The associated tilting frontogenesis had weakened in the same interval yet continued to display a similar distribution relative to the frontal zone as it had 6 h previously. Strong ascent, roughly 18 dPa s^{-1}, was associated with rapid surface cyclogenesis over the eastern Great Lakes, as described by Martin (2006). This pocket of ascent was primarily shearwise omega (Fig. 14b) with some contribution from the transverse ascent (Fig. 14c), located in the left exit region of the jet streak. The subsidence, and associated positive tilting frontogenesis, was comprised of significant contributions from both components of QG omega. Shearwise subsidence contributed the majority of the maxima near the South Dakota/Nebraska border (Fig. 14b), whereas the broad band of subsidence over the Midwest was predominantly associated with transverse omega (Fig. 14c). Vertical cross sections of tilting frontogenesis at this time (not shown) demonstrated a weakening and vertical contraction (to above ~550 hPa) of the frontogenetic signal as compared to prior times.

5. Discussion and Conclusions

Though upper-level fronts are known to develop in both northwesterly and

southwesterly flow, the most intense upper frontogenesis events take place in northwesterly flow where the primary intensification mechanism is differential subsidence (Schultz and Doswell 1999). A particularly favorable synoptic environment within which northwesterly flow upper frontogenesis occurs is one characterized by cold air advection in cyclonic shear. A number of modeling studies based on observed and idealized flows (i.e. Shapiro 1981, Keyser and Pecnick 1985, Keyser et al. 1986, Reeder and Keyser 1988, Rotunno et al. 1994) have shown that cold air advection in cyclonic shear promotes the establishment of a thermally indirect transverse circulation capable of scalar frontogenetic tilting and upper frontogenesis. In most observed cases of northwesterly flow upper frontogenesis, however, cold air advection does not occur along the entire length of the front. In fact, the majority of cases described in the literature exhibit mixed thermal advection along their lengths; cold air advection near the base of the thermal trough but often warm air advection some distance upstream of the thermal trough (Schultz and Doswell 1999). In the present case the thermal advection was nearly entirely positive early in the upper front life cycle (Fig. 15a) with cold air advection developing and becoming further concentrated near the base of the thermal trough as the development proceeded (Figs. 15 b-d). As the cold air advection intensified, so did the contribution of the transverse subsidence to upper frontogenesis as illustrated by consideration of Figs. 7c, 9c, 11c, and 13c. Thus, the mechanism that leads to the initiation and distribution of cold air advection along the front is an important aspect of the upper frontogenesis process.

Rotunno et al. (1994) analyzed normal mode cyclogenesis in a baroclinic primitive

equation channel model to examine the northwesterly flow upper frontogenesis process and mechanisms for the onset of along-front cold air advection. Their analysis focused on subsiding cold air in northwesterly flow between an upstream ridge and downstream trough as the primary mechanism for establishing cold air advection in cyclonic shear. Further clarification concerning the role of subsidence in this regard arises from the analysis of SD99 who showed that an along-isentrope increase in subsidence (i.e. $\frac{\partial \omega}{\partial s} > 0$) promotes cyclonic rotation of $\nabla\theta$ through the tilting contribution to F_s, the rotational frontogenesis function.

The environment surrounding a vorticity maxima in shear flow can be conceptually divided into three regions; one upshear of the maxima, one downshear of the maxima, and one encompassing the maxima as show schematically in Fig. 16. The Sutcliffe (1947)/Trenberth (1978) approximation to the QG ω-equation[3] diagnoses the characteristic distribution of vertical motions in this environment with a subsidence (ascent) maximum upshear (downshear) of the vorticity maximum as illustrated. In the regions upshear and downshear of the vorticity maximum, $\frac{\partial \omega}{\partial s} > 0$ and a cyclonic rotation of $\nabla\theta$ by tilting is implied. In the region encompassing the vorticity maxima, however, $\frac{\partial \omega}{\partial s} < 0$ and anticyclonic rotation via tilting is implied. SD99 showed that the cyclonic rotation of $\nabla\theta$ provided by the vertical vorticity in this region is larger in magnitude than the opposing

[3] Martin (1999) showed that the Sutcliffe (1947)/Trenberth(1978) approximation actually describes twice the effect of the geostrophic relative vorticity on the rotation of $\nabla\theta$.

tendency provided by the tilting. Given the smaller $\left|\frac{\partial \omega}{\partial s}\right|$ in the upshear and downshear regions, the cyclonic rotation of $\nabla\theta$ provided by tilting in those locations is of even smaller magnitude than that in the vicinity of the vorticity maxima. Were the schematic vorticity maxima in Fig. 16 embedded within an upper trough axis, the upshear (downshear) region would be characterized by northwesterly (southwesterly) flow and parcels flowing *toward* the vorticity maxima (i.e. toward the trough axis in northwesterly flow) would experience a systematic *increase* in the forcing for cyclonic rotation of $\nabla\theta$; whereas quite the opposite would apply to those parcels streaming *away* from the vorticity maxima in southwesterly flow. Consequently, it is likely that cold air advection in cyclonic shear will intensify preferentially in northwesterly flow, resulting in more intense and more frequent upper frontogenesis under such circumstances.

Although SD99 established the importance of the rotational frontogenesis process to upper frontogenesis, they were not able to explicitly consider the role that the secondary vertical circulation associated with the rotational frontogenesis might play in the intensification of an upper-level front. By employing the QG vector frontogenesis perspective, the present study specifically considers that vertical circulation, the shearwise circulation, in order to further investigate the role of rotational frontogenesis in the upper front life cycle. The QG rotational frontogenesis is represented by the along-isentrope component of $\boldsymbol{Q}$, $\boldsymbol{Q_s}$. When $\boldsymbol{Q_s}$ is directed along (opposite) the geostrophic vertical shear, cyclonic (anticyclonic) rotation of $\nabla\theta$ is implied. The divergence of $\boldsymbol{Q_s}$ diagnoses the

vertical circulation associated with the given rotational frontogenesis. In the case of positive rotational frontogenesis (i.e. cyclonic rotation of $\nabla\theta$) a dipole of vertical motion with ascent downshear of the descent is diagnosed. The persistent positive rotational frontogenesis in the vicinity of the geopotential trough axis in this case was associated with an upstream subsidence maximum that consistently contributed the largest share of the scalar tilting frontogenesis involved in the intensification of this upper front.

Thus, a synthesis of prior results with the present analysis suggests that the contributions of rotational frontogenesis to upper-level frontogenesis during the upper frontal life cycle are twofold. First, as demonstrated by SD99, the rotational frontogenesis provides forcing for cyclonic rotation of $\nabla\theta$ near the base of the geopotential trough (more generally the relative vorticity maximum) thereby enhancing the Shapiro effect by means of intensifying the cold air advection in cyclonic shear. Second, as shown here, the rotational frontogenesis is itself associated with a vertical circulation (the shearwise circulation) that persistently and significantly contributes to frontogenetic tilting. The superposition of the transverse and shearwise subsidence maxima, associated with the Shapiro effect and the rotational frontogenesis that enhances the Shapiro effect, respectively, lead to a period of rapid upper frontogenesis in the present case. Whether or not the set of circumstances outlined here is characteristic of the comprehensive life cycle of upper tropospheric jet/front systems is clearly an outstanding question of great scientific and operational relevance.

The dominance of the shearwise contribution to the early stages of northwesterly flow upper frontogenesis in the present analysis is reminiscent of the primacy of shearwise

updrafts in the cyclogenetic stage of the extratropical cyclone life cycle as described by Martin (2006, 2007). In those studies, as in this one, the contributions of the transverse vertical motions to the processes in question gradually increased as frontal structures began to take shape. This similarity suggests that the shearwise vertical motions, what Keyser et al. (1992) referred to as wave scale vertical motions, and the associated process of rotational frontogenesis play a primary role in molding the large scale flow into some of the basic synoptic scale structures involved in the production of sensible weather in the extratropics.

REFERENCES

Barnes, S. L., F. Caracena, and A. Marroquin, 1996: Extracting synoptic-scale diagnostic information from mesoscale models: The Eta model, gravity waves, and quasigeostrophic diagnostics. *Bull. Amer. Meteor. Soc*., **77**, 519-528.

Eliassen, A., 1962: On the vertical circulation in frontal zones. *Geofys. Publ.*, **24**(4), 147-160.

Hoskins, B. J., I. Draghici, and H. C. Davies, 1978: A new look at the ω-equation. *Quart. J. Roy. Meteo. Soc*., **104**, 31-38.

Keyser, D. and M. J. Pecnick, 1985: A two-dimensional primitive equation model of frontogenesis forced by confluence and horizontal shear. *J. Atmos. Sci.*, **42**, 1259-1282.

_____ and M. A. Shapiro, 1986: A review of the structure and dynamics of upper-level frontal zones. *Mon. Wea. Rev.,* **114**, 452-499.

_____, M. J. Reeder, and R. J. Reed, 1988: A generalization of Petterssen's frontogenesis function and its relation to the forcing of vertical motion. *Mon. Wea. Rev.* **116**, 762-780.

_____, B. D. Schmidt and D. G Duffy, 1992: Quasigeostrophic vertical motions diagnosed from along- and cross-isentrope components of the ***Q*** vector. *Mon. Wea. Rev.,* **120(**5), 731–741.

Martin, J. E., 1999: Quasigeostrophic forcing of ascent in the occluded sector of cyclones and the trowal airstream. *Mon. Wea. Rev.* **127**, 70-88.

_____, 2006: The role of shearwise and transverse quasigeostrophic vertical motions in the midlatitude cyclone life cycle. *Mon. Wea. Rev.* **134**, 1174–1193.

_____, 2007: Lower-tropospheric height tendencies associated with the shearwise and transverse components of quasigeostropic vertical motion. *Mon. Wea. Rev.* **135**, 2803–2809.

Palmén, E. and K. M. Nagler, 1949: The formation and structure of large-scale disturbances in the westerlies. *J. of Meteor.,* **6**(4), 227-242.

Petterssen, S., 1936: Contribution to the theory of frontogenesis. *Geofys. Publ.*, **11**(6), 1-27.

Reed. R. J., 1955: A study of a characteristic type of upper-level frontogenesis. *J. Meteor.*, **12**, 226-237.

_____ and F. Sanders, 1953: An investigation of the development of a mid-tropospheric frontal zone and its associated vorticity field. *J. Meteor.*, **10**, 338-349.

Reeder, M. J. and D. Keyser, 1988: Balanced and unbalanced upper-level frontogenesis. *J. Atmos. Sci.* **45(**22), 3366–3386.

Rotunno, R., W. C. Skamarock, and C. Snyder, 1994: An analysis of frontogenesis in numerical simulations of baroclinic waves. J. Atmos. Sci., 51, 3373-3398.

Sawyer, J. S., 1956: The vertical circulation at meteorological fronts and its relation to frontogenesis. *Proc. Roy. Soc. London*, **A234**, 346-362.

Schultz, D. M. and C. A. Doswell, 1999: Conceptual models of upper-level frontogenesis in south-westerly and north-westerly flow. *Quart. J. Roy. Meteor. Soc*, **125**, 2535-2562.

_____, and F. Sanders, 2002: Upper-level frontogenesis associated with the birth of mobile troughs in northwesterly flow. *Mon. Wea. Rev*., **130**, 2593-2610.

Shapiro, M. A., 1981: Frontogenesis and geostrophically forced secondary circulations in the vicinity of jet stream-frontal zone systems. *J. Atmos. Sci.*, **38**, 954-973.

Sutcliffe, R. C., 1947: A contribution to the problem of development. Quart. J. Roy. Meteor. Soc., 73, 370-383.

Trenberth, K. E., 1978: On the interpretation of the quasigeostrophic omega equation. *Mon. Wea. Rev*., **106**, 1321-137.

FIGURE CAPTIONS

Fig. 1 (a) 400 hPa geopotential height (solid lines), potential temperature (dashed) and absolute vorticity (shading) from the Eta model analysis valid at 1200 UTC 11 November 2003. Geopotential height is labeled in m and contoured every 120 m. Isentropes are labeled in K and contoured every 4 K. Absolute vorticity labeled in units of 10^{-5} s^{-1} and shaded every 5 x 10^{-5} s^{-1} beginning at 15 x 10^{-5} s^{-1}. (b) 300 hPa geopotential height (solid lines) and isotachs (shaded) from the Eta model analysis valid at 1200 UTC 11 November 2003. Geopotential height labeled as in Fig. 1a and contoured every 200 m. Isotachs labeled in m s^{-1} and shaded every 10 m s^{-1} beginning at 40 m s^{-1}.

Fig. 2 (a) As for Fig. 1a but from the Eta model analysis valid at 0000 UTC 12 November 2003. (b) As for Fig. 1b but from the Eta model analysis valid at 0000 UTC 12 November 2003.

Fig. 3 (a) As for Fig. 1a but from the Eta model analysis valid at 1200 UTC 12 November 2003. (b) As for Fig. 1b but from the Eta model analysis valid at 1200 UTC 12 November 2003.

Fig. 4 (a) As for Fig. 1a but from the Eta model analysis valid at 1800 UTC 12 November 2003. (b) As for Fig. 1b but from the Eta model analysis valid at 1800 UTC 12 November 2003.

Fig. 5 (a) As for Fig. 1a but from the Eta model analysis valid at 0000 UTC 13 November

2003. (b) As for Fig. 1b but from the Eta model analysis valid at 0000 UTC 13 November 2003.

Fig. 6 (a) 400 hPa isentropes, $\boldsymbol{Q}$-vectors, total QG vertical motions (ω_{tot}), and tilting frontogenesis calculated using ω_{tot} from the Eta model analysis valid at 1200 UTC 11 November 2003. Thin solid lines are isentropes, labeled in K and contoured every 3K. Thick solid (dashed) lines are positive (negative) ω_{tot} labeled in dPa s^{-1} and contoured every 2 (-2) dPa s^{-1} beginning at 2 (-2) dPa s^{-1}. Tilting frontogenesis is in units of K m^{-1} s^{-1} and contoured every 8 (-8) x 10^{-9} K m^{-1} s^{-1} starting at 8 (-8) x 10^{-9} K m^{-1} s^{-1} with dark (light) shading indicating positive (negative) tilting frontogenesis. Vertical cross-sections along line A-A` shown in Fig. 7.

(b) As for Fig. 6a but with $\boldsymbol{Q_s}$ vectors, shearwise QG vertical motions (ω_s), and tilting frontogenesis calculated using ω_s from the Eta model analysis valid at 1200 UTC 11 November 2003. Tilting frontogenesis contoured in units of 4 (-4) x 10^{-9} K m^{-1} s^{-1} beginning at 4 (-4) x 10^{-9} K m^{-1} s^{-1}.

(c) As for Fig. 6a but with $\boldsymbol{Q_n}$ vectors, transverse QG vertical motions (ω_n), and tilting frontogenesis calculated using ω_n from the Eta model analysis valid at 1200 UTC 11 November 2003. Tilting frontogenesis labeled, contoured and shaded as in Fig. 6b.

Fig. 7 (a) Vertical cross section, along line A-A` in Fig. 6a, of isotachs, isentropes, ω_{tot}, and tilting frontogenesis calculated with ω_{tot} from the Eta model analysis valid at 1200 UTC 11 November 2003. Thin dashed lines are isotachs labeled in m s^{-1} and

contoured every 10 m s^{-1} starting at 40 m s^{-1}. Uppercase "J" indicates the location of the jet core. Isentropes labeled and contoured as in Fig. 6a. Thick solid (dashed) lines are positive (negative) ω_{tot} labeled in dPa s^{-1} and contoured every 2 (-2) dPa s^{-1} beginning at 2 (-2) dPa s^{-1} but including the 1 (-1) dPa s^{-1} contour as well. Positive (negative) tilting frontogenesis is darkly (lightly) shaded and contoured every 3 (-3) x 10^{-9} K m^{-1} s^{-1} beginning at 3 (-3) x 10^{-9} K m^{-1} s^{-1}.

(b) As for Fig. 7a but with ω_s and tilting frontogenesis calculated using ω_s. Variables labeled, contoured, and shaded as in Fig. 7a. (c) As for Fig. 7a but with ω_n and tilting frontogenesis calculated using ω_n, Variables labeled, contoured, and shaded as in Fig. 7a.

Fig. 8 (a) As for Fig. 6a but from the Eta model analysis valid at 0000 UTC 12 November 2003. Vertical cross-sections along line B-B` shown in Fig. 9. (b) As for Fig. 6b but from the Eta model analysis valid at 0000 UTC 12 November 2003. (c) As for Fig. 6c but from the Eta model analysis valid at 0000 UTC 12 November 2003.

Fig. 9 (a) Vertical cross-section along line B-B` in Fig. 8a. As for Fig. 7a but from the Eta model analysis valid at 0000 UTC 12 November 2003. (b) As for Fig. 7b but from the Eta model analysis valid at 0000 UTC 12 November 2003. (c) as For Fig. 7c but from the Eta model analysis valid at 0000 UTC 12 November 2003.

Fig. 10 (a) As for Fig. 6a but from the Eta model analysis valid at 1200 UTC 12 November 2003. Vertical cross-sections along line C-C` shown in Fig. 11. (b) As for Fig. 6b but

from the Eta model analysis valid at 1200 UTC 12 November 2003. (c) As for Fig. 6c but from the Eta model analysis valid at 1200 UTC 12 November 2003.

Fig. 11 (a) Vertical cross-section along line C-C` in Fig. 10a. As for Fig. 7a but from the Eta model analysis valid at 1200 UTC 12 November 2003. Tilting frontogenesis is contoured every 6 (-6) x 10^{-9} K m^{-1} s^{-1} beginning at 6 (-6) x 10^{-9} K m^{-1} s^{-1}. (b) As for Fig. 7b but from the Eta model analysis valid at 1200 UTC 12 November 2003. Tilting frontogenesis contoured and shaded as in Fig. 11a. (c) As for Fig. 7c but from the Eta model analysis valid at 1200 UTC 12 November 2003. Tilting frontogenesis is contoured and shaded as in Fig. 11a.

Fig. 12 (a) As for Fig. 6a but from the Eta model analysis valid at 1800 UTC 12 November 2003. Vertical cross-sections along line D-D` shown in Fig. 13. (b) As for Fig. 6b but from the Eta model analysis valid at 1800 UTC 12 November 2003. (c) As for Fig. 6c but from the Eta model analysis valid at 1800 UTC 12 November 2003.

Fig. 13 (a) Vertical cross-section along line D-D` in Fig. 12a. As for Fig. 11a but from the Eta model analysis valid at 1800 UTC 12 November 2003. (b) As for Fig. 11b but from the Eta model analysis valid at 1800 UTC 12 November 2003. (c) As for Fig. 11c but from the Eta model analysis valid at 1800 UTC 12 November 2003.

Fig. 14 (a) As for Fig. 6a but from the Eta model analysis valid at 0000 UTC 13 November 2003. (b) As for Fig. 6b but from the Eta model analysis valid at 0000 UTC 13

November 2003. (c) As for Fig. 6c but from the Eta model analysis valid at 0000 UTC 13 November 2003.

Fig. 15 (a) 400 hPa geopotential height (solid lines), isentropes (dashed lines) and geostrophic temperature advection (shading) from the Eta model analysis valid at 1200 UTC 11 November 2003. Geopotential height labeled in m and contoured every 120 m. Isentropes labeled and contoured as in Fig. 6a. Dark (light) shading represents negative (positive) geostrophic temperature advection labeled in units of K s^{-1} and contoured every –2 (2) x 10^{-4} K s^{-1} beginning at –2 (2) x 10^{-4} K s^{-1}. (b) As for Fig. 15a but from the Eta model analysis valid at 0000 UTC 12 November 2003. (c) As for Fig. 15a but from the Eta model analysis valid at 1200 UTC 12 November 2003. (d) As for Fig. 15a but from the Eta model analysis valid at 0000 UTC 13 November 2003.

Fig. 16 Schematic illustrating the mechanisms by which positive rotational frontogenesis is induced in the vicinity of an isolated vertical vorticity maxima. Dark shaded oval represents the vertical vorticity maxima. Black arrows are the associated $\boldsymbol{Q_s}$ vectors. Thin dashed lines are isentropes. Convergence (divergence) of $\boldsymbol{Q_s}$ downshear (upshear) of the vorticity maxima is associated with ascent (descent) indicated by the thick solid (dashed) lines. Lightly shaded regions upshear and downshear of the vorticity maxima are characterized by positive rotational frontogenesis induced by along-shear tilting (i.e. $\frac{\partial \omega}{\partial s} > 0$). In the unshaded center region, $\frac{\partial \omega}{\partial s} < 0$ and positive rotational frontogenesis is forced instead by cyclonic rotation associated with the

vertical vorticity maxima. See text for additional explanation.

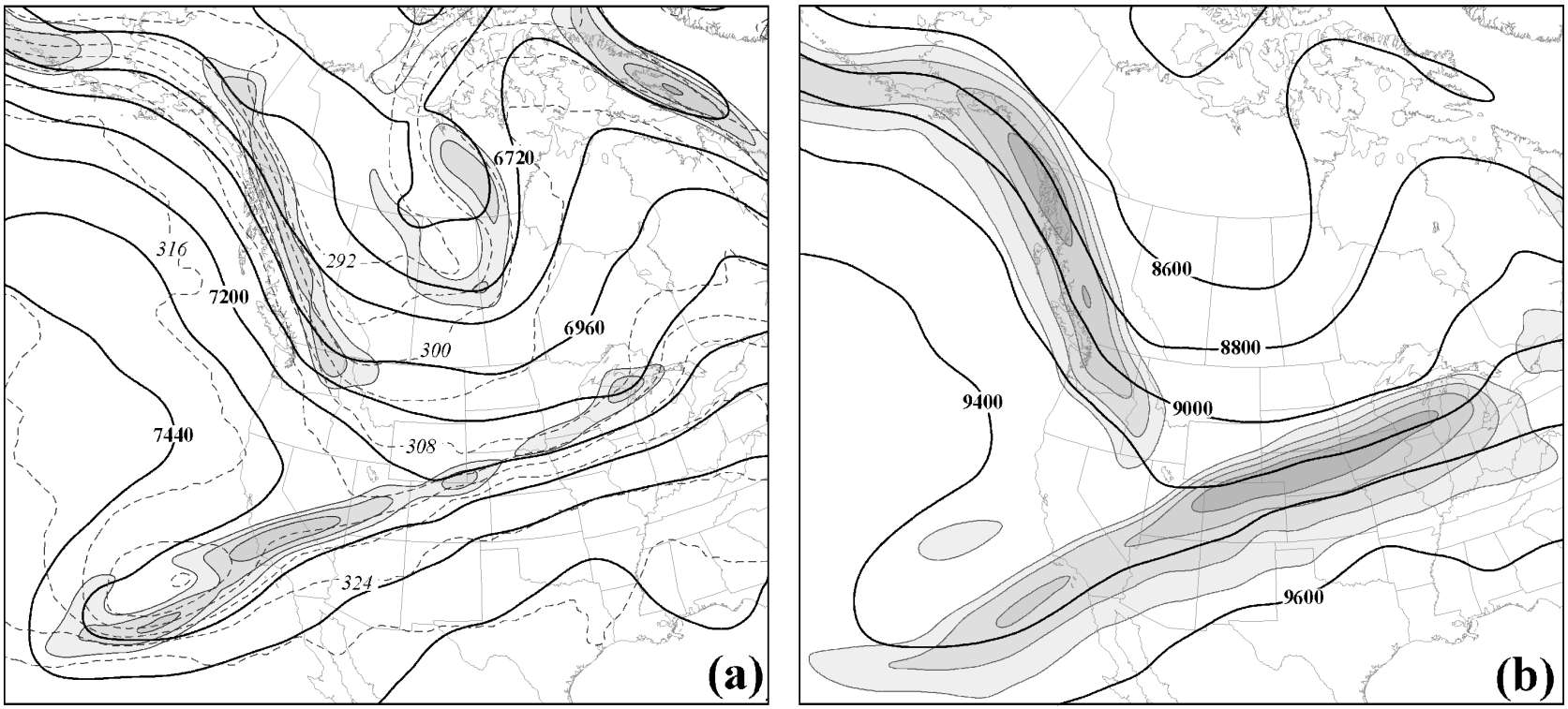

Fig. 1 (a) 400 hPa geopotential height (solid lines), potential temperature (dashed) and absolute vorticity (shading) from the Eta model analysis valid at 1200 UTC 11 November 2003. Geopotential height is labeled in m and contoured every 120 m. Isentropes are labeled in K and contoured every 4 K. Absolute vorticity labeled in units of 10^{-5} s^{-1} and shaded every 5 x 10^{-5} s^{-1} beginning at 15 x 10^{-5} s^{-1} (b) 300 hPa geopotential height (solid lines) and isotachs (shaded) from the Eta model analysis valid at 1200 UTC 11 November 2003. Geopotential height labeled as in Fig. 1a and contoured every 200 m. Isotachs labeled in m s^{-1} and shaded every 10 m s^{-1} beginning at 40 m s^{-1}.

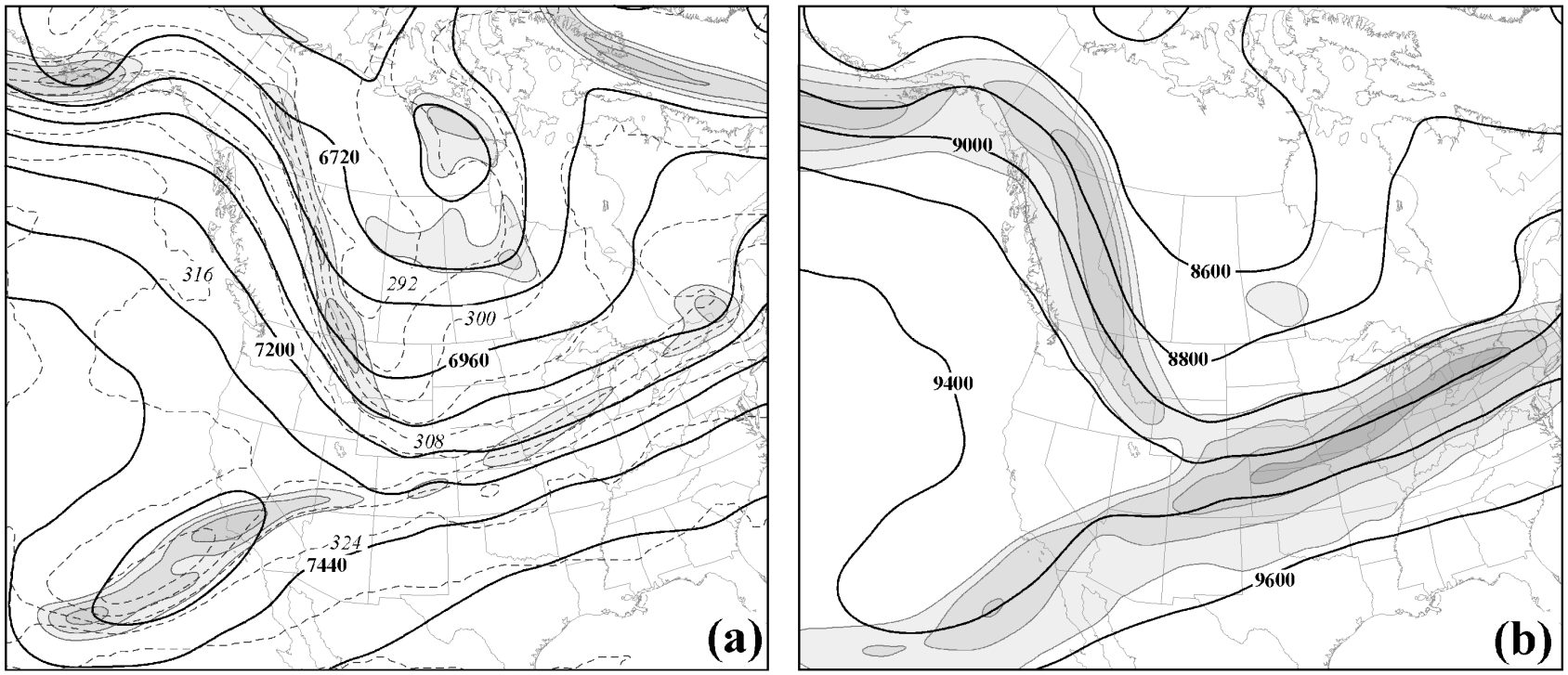

Fig. 2 (a) As for Fig. 1a but from the Eta model analysis valid at 0000 UTC 12 November 2003. (b) As for Fig. 1b but from the Eta model analysis valid at 0000 UTC 12 November 2003.

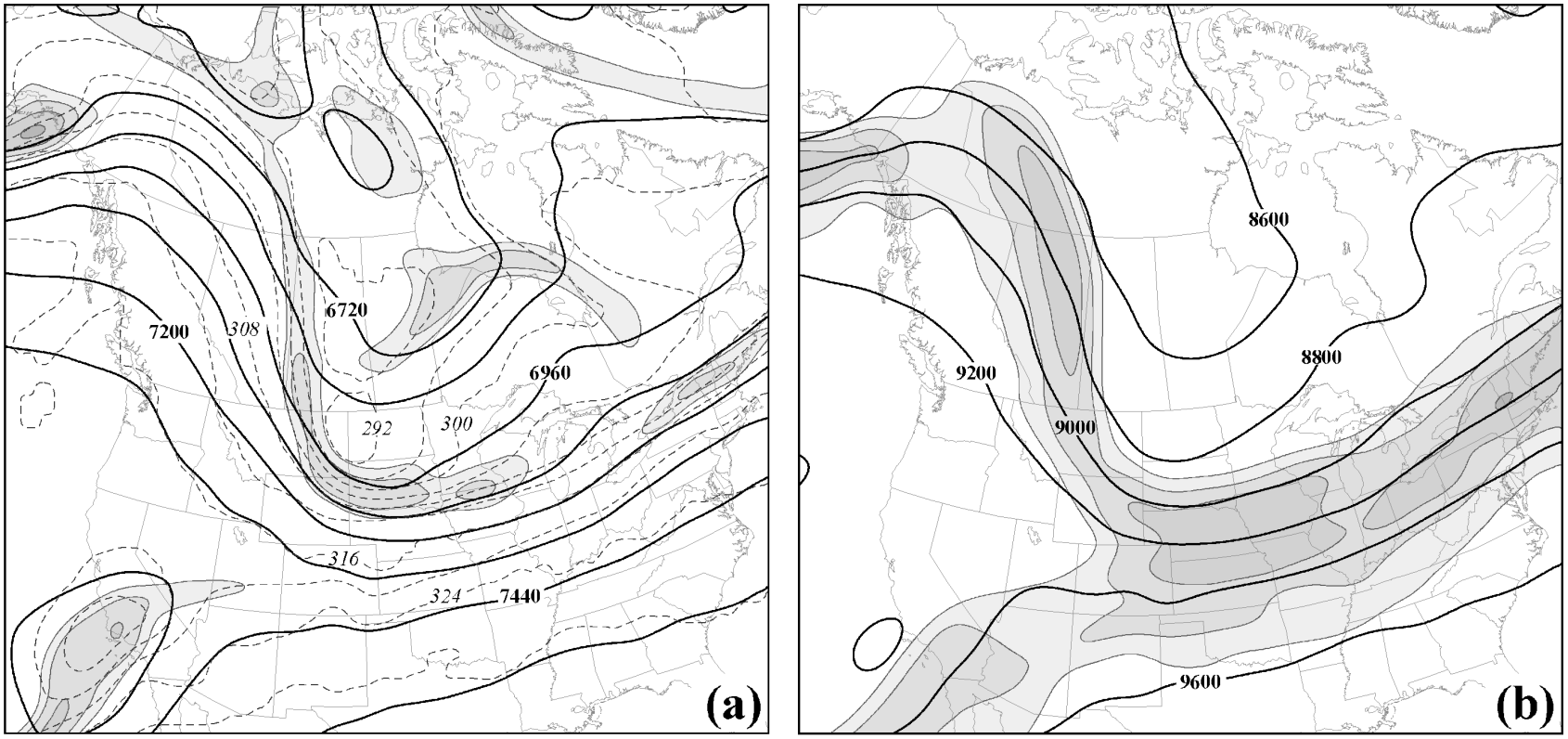

Fig. 3 (a) As for Fig. 1a but from the Eta model analysis valid at 1200 UTC 12 November 2003. (b) As for Fig. 1b but from the Eta model analysis valid at 1200 UTC 12 November 2003.

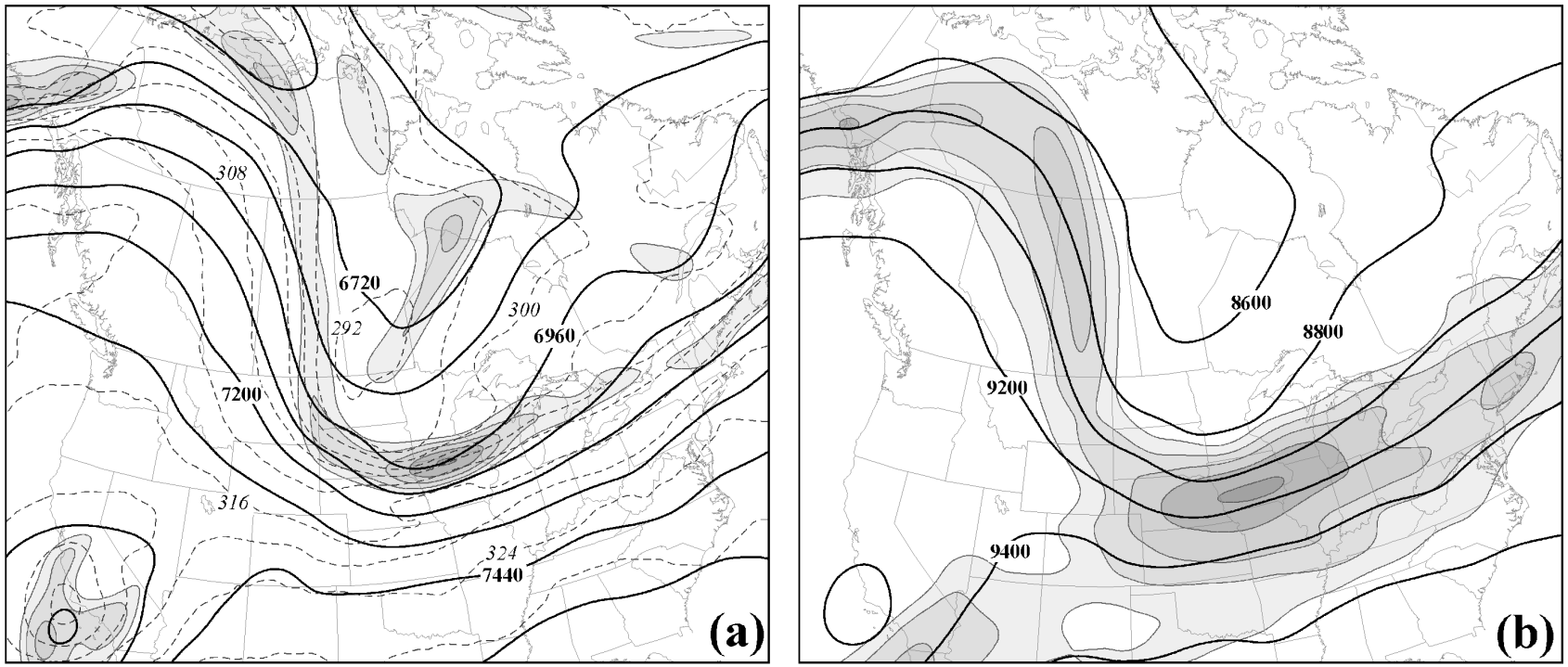

Fig. 4 (a) As for Fig. 1a but from the Eta model analysis valid at 1800 UTC 12 November 2003. (b) As for Fig. 1b but from the Eta model analysis valid at 1800 UTC 12 November 2003.

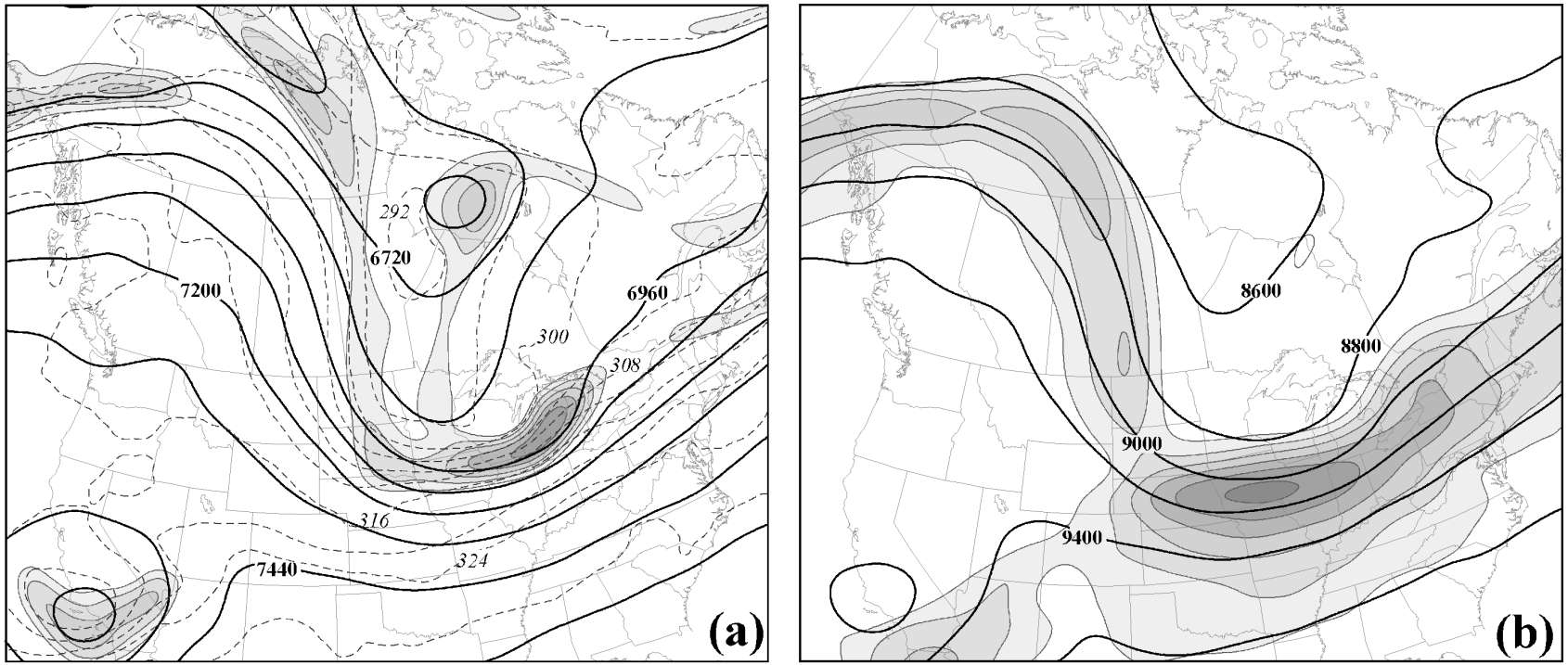

Fig. 5 (a) As for Fig. 1a but from the Eta model analysis valid at 0000 UTC 13 November 2003. (b) As for Fig. 1b but from the Eta model analysis valid at 0000 UTC 13 November 2003.

Fig. 6 (a) 400 hPa isentropes, ***Q***-vectors, total QG vertical motions (ω_{tot}), and tilting frontogenesis calculated using ω_{tot} from the Eta model analysis valid at 1200 UTC 11 November 2003. Thin solid lines are isentropes, labeled in K and contoured every 3K. Thick solid (dashed) lines are positive (negative) ω_{tot} labeled in dPa $s^{-1}$and contoured every 2 (-2) dPa s^{-1} beginning at 2 (-2) dPa s^{-1}. Tilting frontogenesis is in units of K m^{-1} s^{-1} and contoured every 8 (-8) x 10^{-9} K m^{-1} s^{-1} starting at 8 (-8) x 10^{-9} K m^{-1} s^{-1} with dark (light) shading indicating positive (negative) tilting frontogenesis. Vertical cross-sections along line A-A` shown in Fig. 7. (b) As for Fig. 6a but with $\boldsymbol{Q_s}$ vectors, shearwise QG vertical motions (ω_s), and tilting frontogenesis calculated using ω_s from the Eta model analysis valid at 1200 UTC 11 November 2003. Tilting frontogenesis contoured in units of 4 (-4) x 10^{-9} K m^{-1} s^{-1} beginning at 4 (-4) x 10^{-9} K m^{-1} s^{-1}. (c) As for Fig. 6a but with $\boldsymbol{Q_n}$ vectors, transverse QG vertical motions (ω_n), and tilting frontogenesis calculated using ω_n from the Eta model analysis valid at 1200 UTC 11 November 2003. Tilting frontogenesis labeled, contoured and shaded as in Fig. 6b.

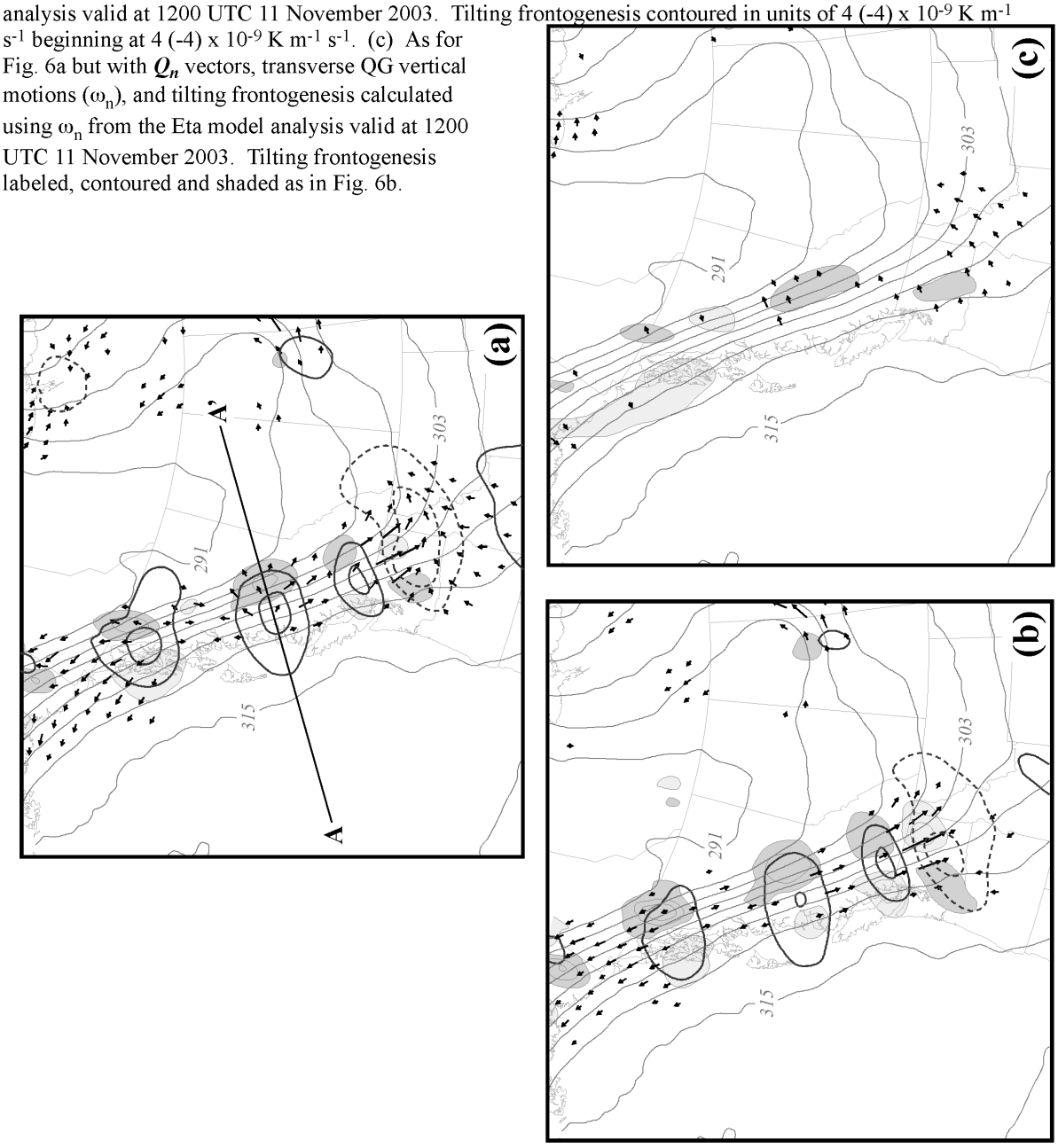

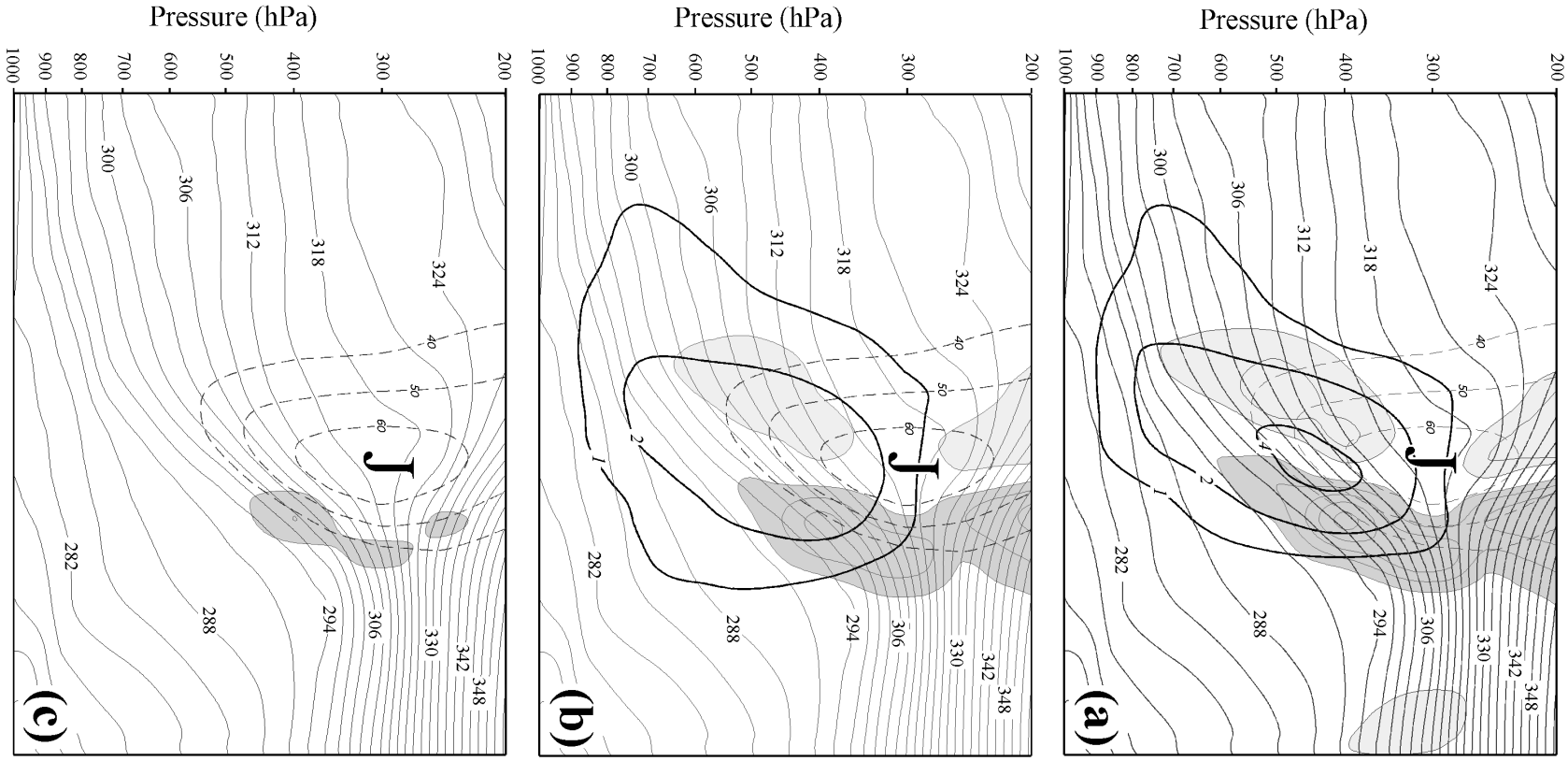

Fig. 7 (a) Vertical cross section, along line A-A` in Fig. 6a, of isotachs, isentropes, ω_{tot}, and tilting frontogenesis calculated with ω_{tot} from the Eta model analysis valid at 1200 UTC 11 November 2003. Thin dashed lines are isotachs labeled in m s^{-1} and contoured every 10 m s^{-1} starting at 40 m s^{-1}. Uppercase " J" indicates the location of the jet core. Isentropes labeled and contoured as in Fig. 6a. Thick solid (dashed) lines are positive (negative) ω_{tot} labeled in dPa s^{-1} and contoured every 2 (-2) dPa s^{-1} beginning at 2 (-2) dPa s^{-1} but including the 1 (-1) dPa s^{-1} contour as well. Positive (negative) tilting frontogenesis is darkly (lightly) shaded and contoured every 3 (-3) x 10^{-9} K m^{-1} s^{-1} beginning at 3 (-3) x 10^{-9} K m^{-1} s^{-1}. (b) As for Fig. 7a but with ω_s and tilting frontogenesis calculated using ω_s. Variables labeled, contoured, and shaded as in Fig. 7a. (c) As for Fig. 7a but with ω_n and tilting frontogenesis calculated using ω_n, Variables labeled, contoured, and shaded as in Fig. 7a.

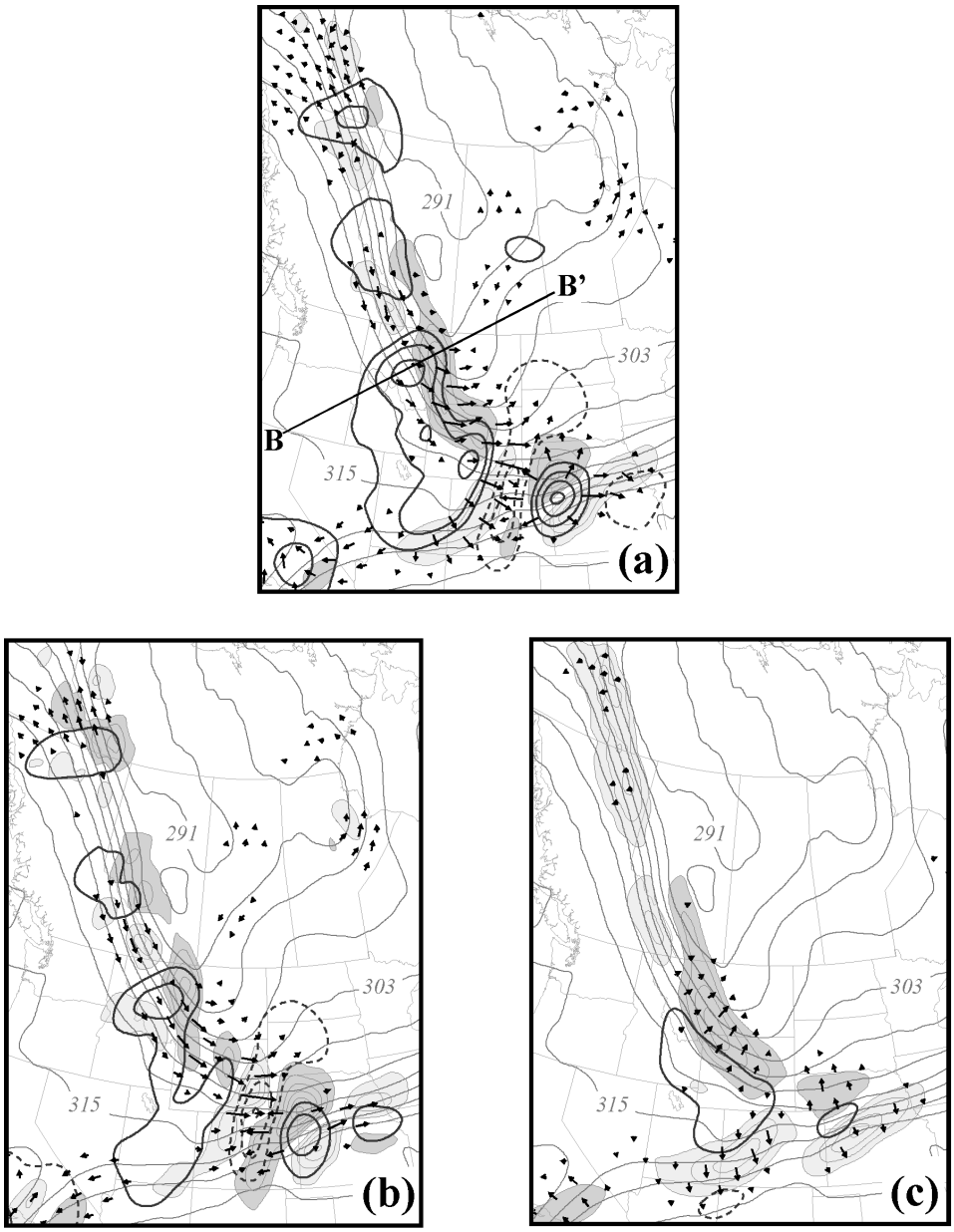

Fig. 8 (a) As for Fig. 6a but from the Eta model analysis valid at 0000 UTC 12 November 2003. Vertical cross-sections along line B-B` shown in Fig. 9. (b) As for Fig. 6b but from the Eta model analysis valid at 0000 UTC 12 November 2003. (c) As for Fig. 6c but from the Eta model analysis valid at 0000 UTC 12 November 2003.

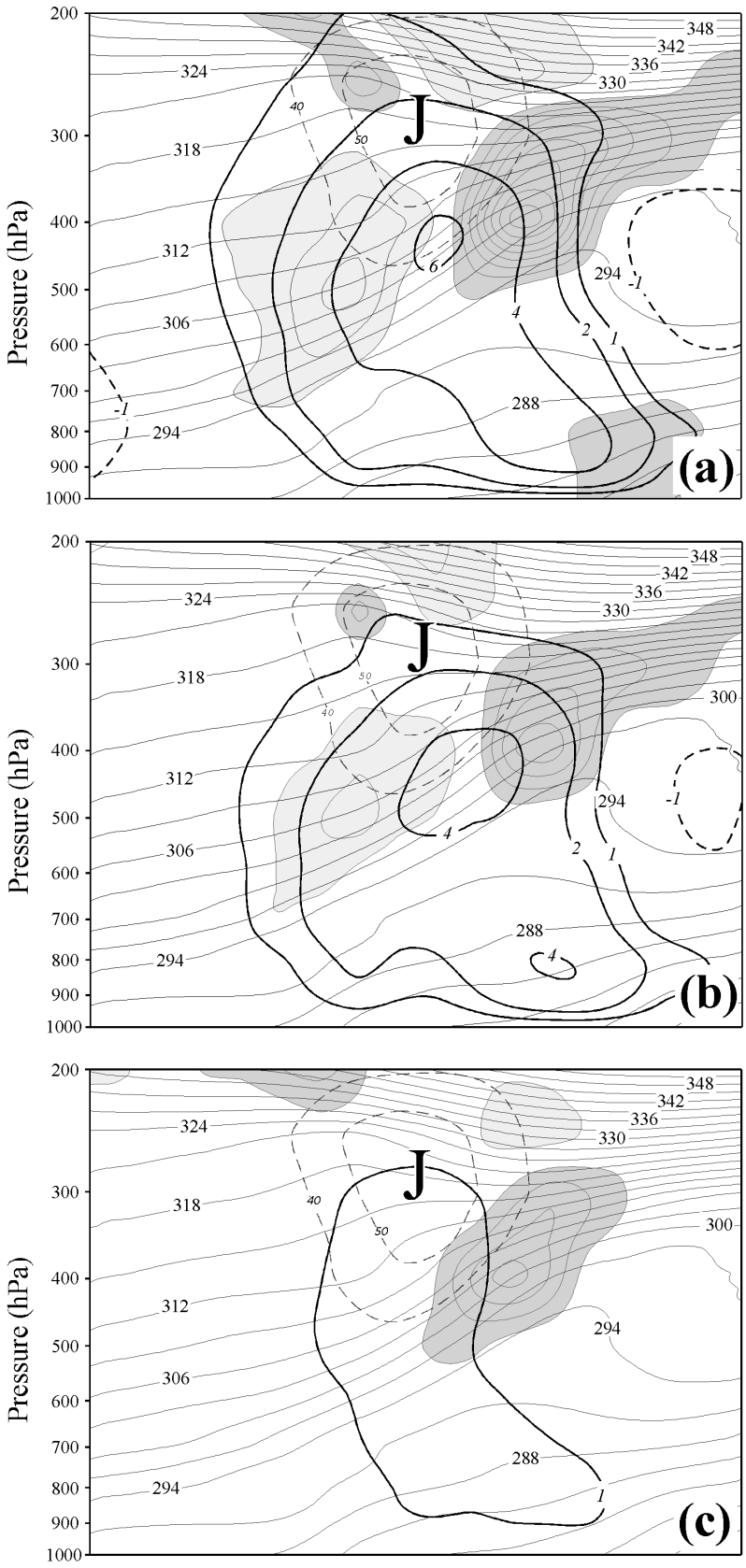

Fig. 9 (a) Vertical cross-section along line B-B` in Fig. 8a. As for Fig. 7a but from the Eta model analysis valid at 0000 UTC 12 November 2003. (b) As for Fig. 7b but from the Eta model analysis valid at 0000 UTC 12 November 2003. (c) as For Fig. 7c but from the Eta model analysis valid at 0000 UTC 12 November 2003.

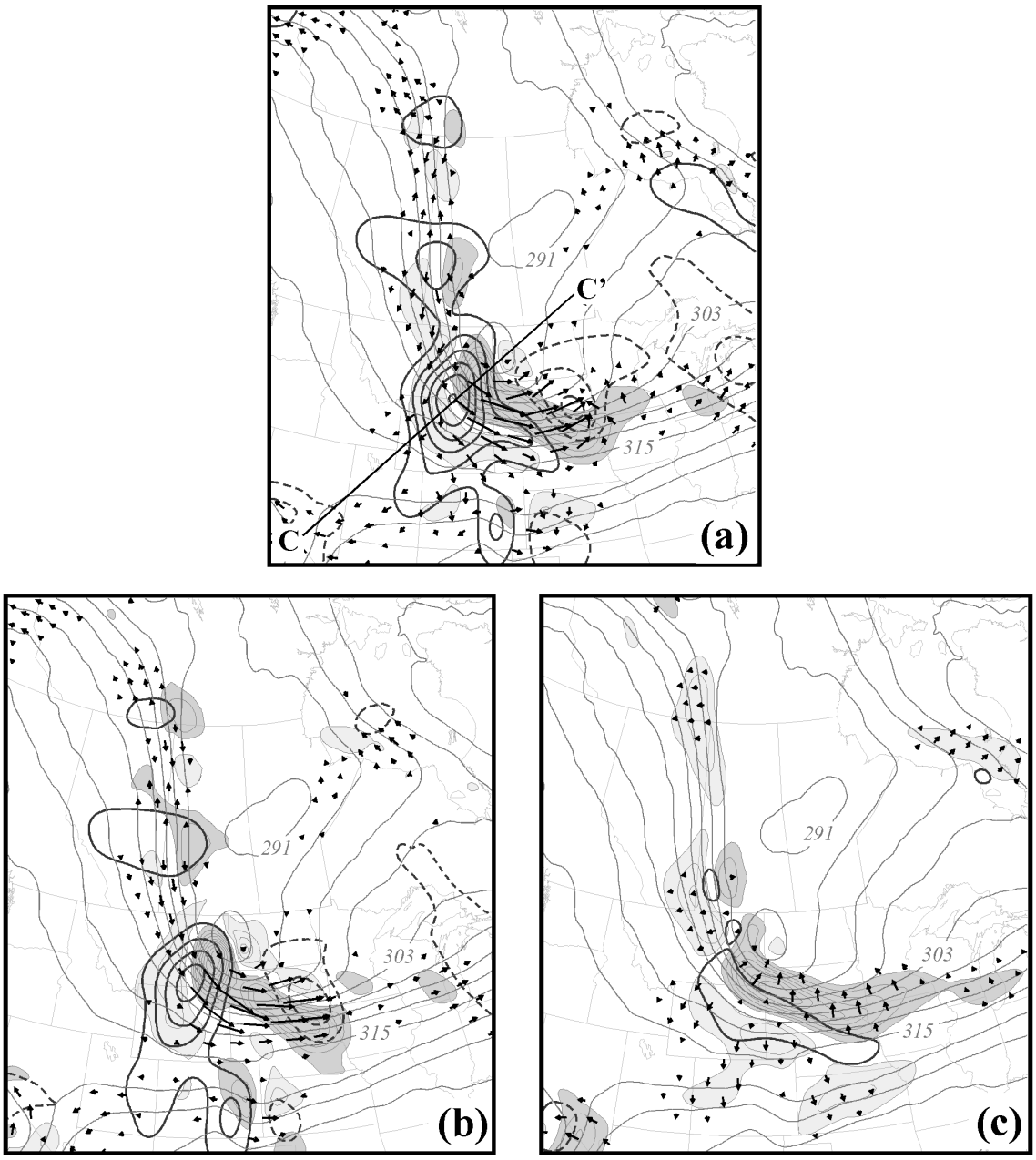

Fig. 10 (a) As for Fig. 6a but from the Eta model analysis valid at 1200 UTC 12 November 2003. Vertical cross-sections along line C-C` shown in Fig. 11. (b) As for Fig. 6b but from the Eta model analysis valid at 1200 UTC 12 November 2003. (c) As for Fig. 6c but from the Eta model analysis valid at 1200 UTC 1 2 November 2003.

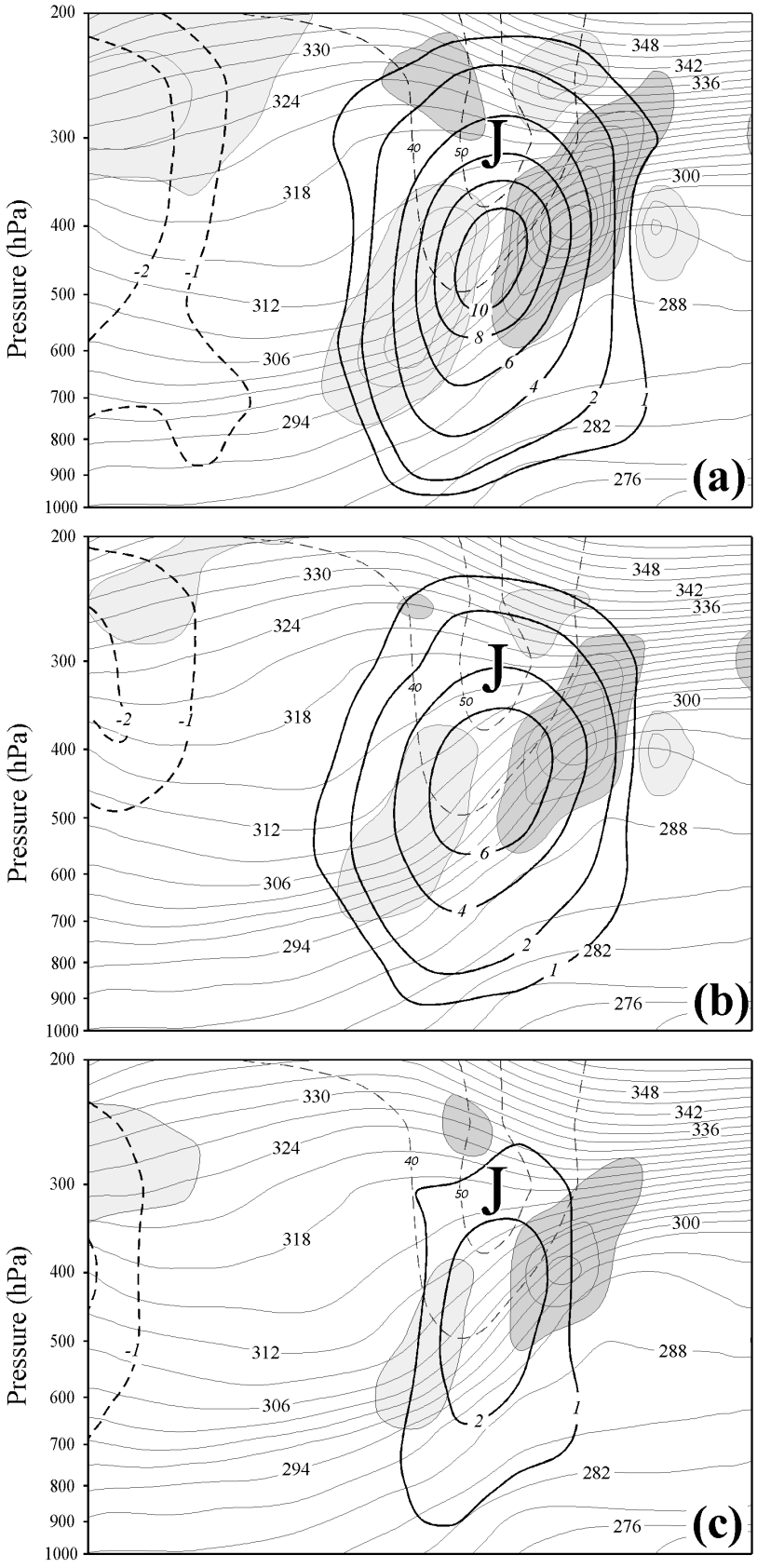

Fig. 11 (a) Vertical cross-section along line C-C` in Fig. 10a. As for Fig. 7a but from the Eta model analysis valid at 1200 UTC 12 November 2003. Tilting frontogenesis is contoured every 6 (-6) x 10^{-9} K m^{-1} s^{-1} beginning at 6 (-6) x 10^{-9} K m^{-1} s^{-1}. (b) As for Fig. 7b but from the Eta model analysis valid at 1200 UTC 12 November 2003. Tilting frontogenesis contoured and shaded as in Fig. 11a. (c) As for Fig. 7c but from the Eta model analysis valid at 1200 UTC 12 November 2003. Tilting frontogenesis is contoured and shaded as in Fig. 11a.

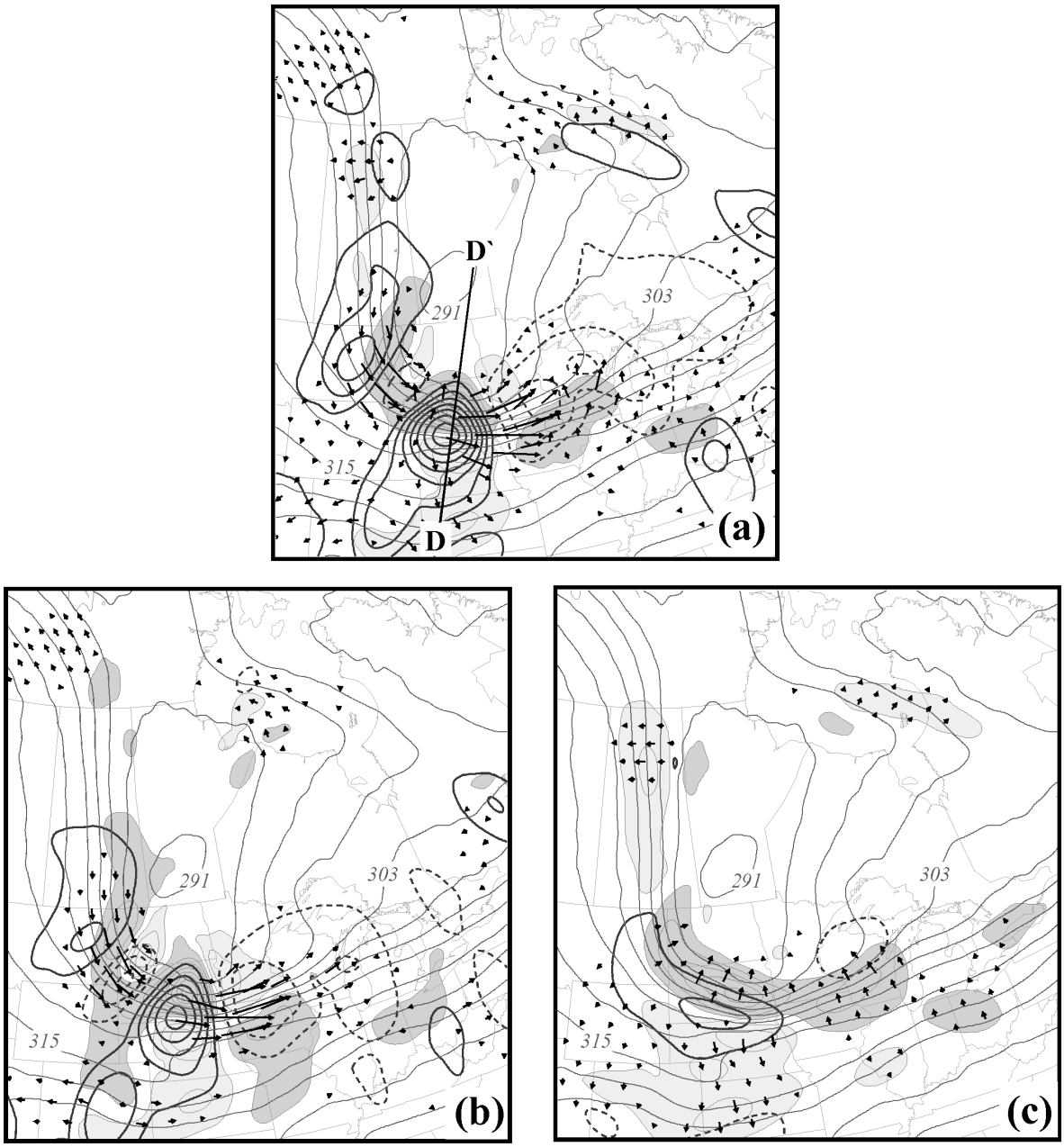

Fig. 12 (a) As for Fig. 6a but from the Eta model analysis valid at 1800 UTC 12 November 2003. Vertical cross-sections along line D-D` shown in Fig. 13. (b) As for Fig. 6b but from the Eta model analysis valid at 1800 UTC 12 November 2003. (c) As for Fig. 6c but from the Eta model analysis valid at 1800 UTC 12 November 2003.

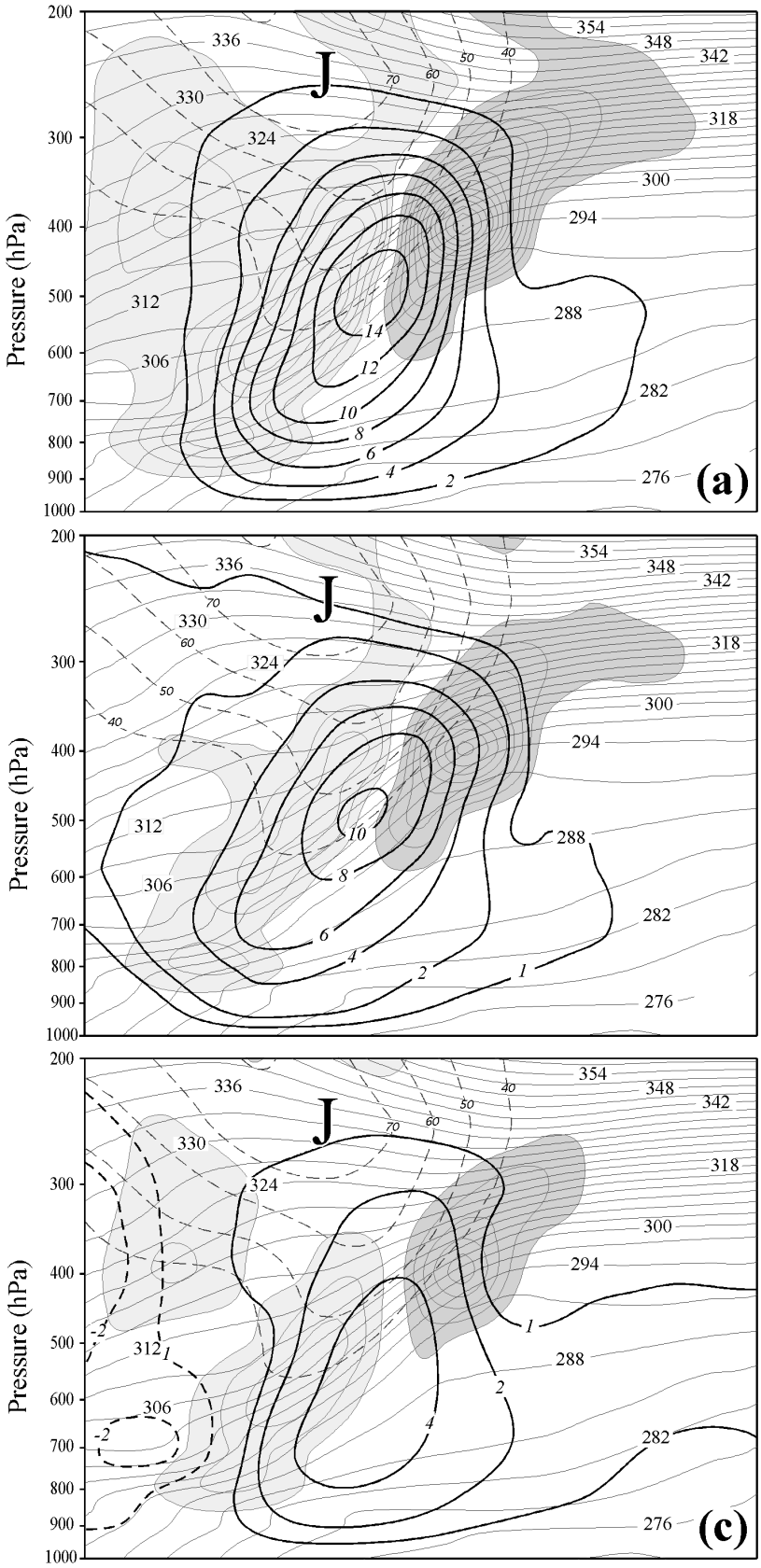

Fig. 13 (a) Vertical cross-section along line D-D` in Fig. 12a. As for Fig. 11a but from the Eta model analysis valid at 1800 UTC 12 November 2003. (b) As for Fig. 11b but from the Eta model analysis valid at 1800 UTC 12 November 2003. (c) As for Fig. 11c but from the Eta model analysis valid at 1800 UTC 12 November 2003.

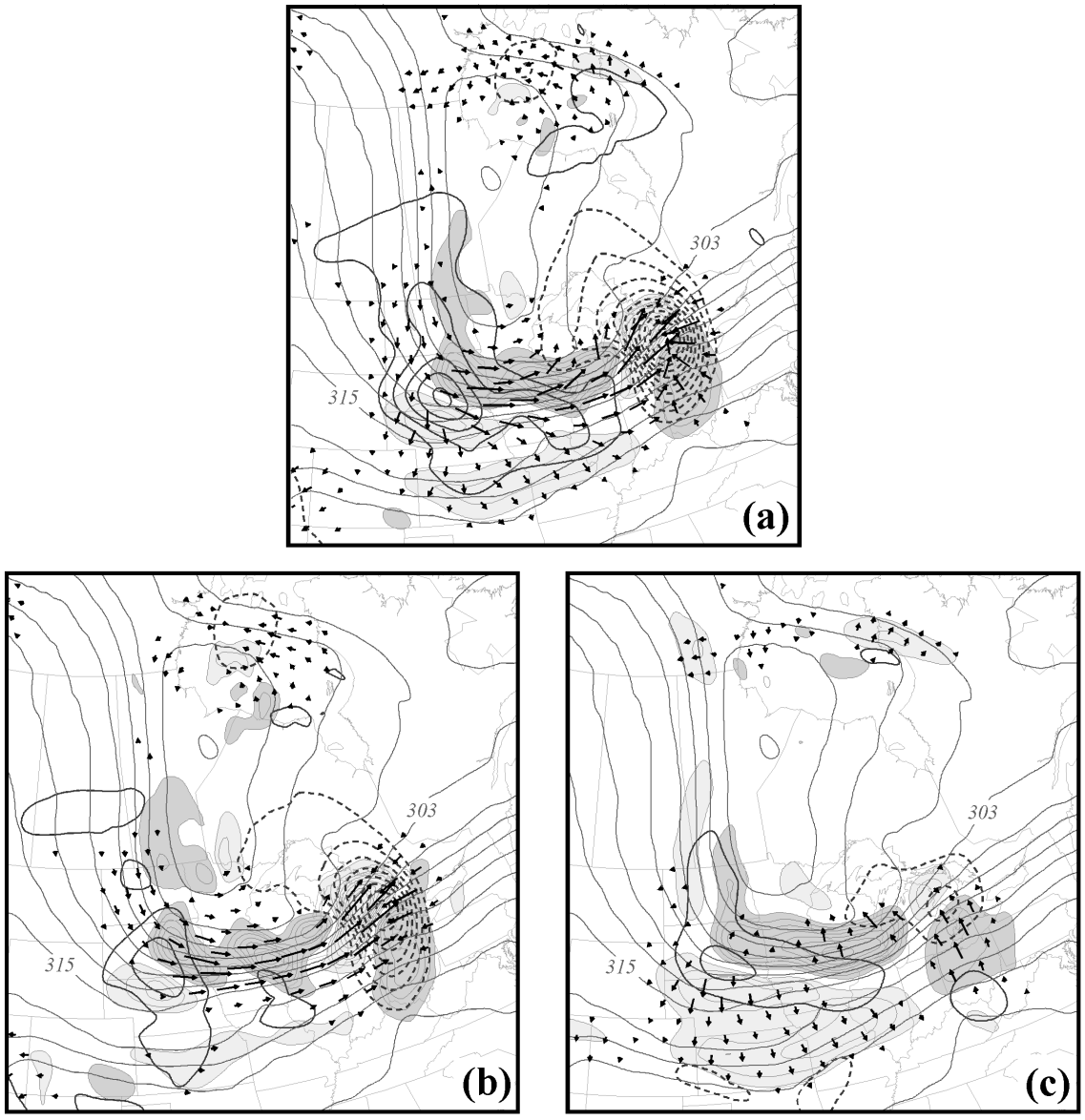

Fig. 14 (a) As for Fig. 6a but from the Eta model analysis valid at 0000 UTC 13 November 2003. (b) As for Fig. 6b but from the Eta model analysis valid at 0000 UTC 13 November 2003. (c) As for Fig. 6c but from the Eta model analysis valid at 0000 UTC 13 November 2003.

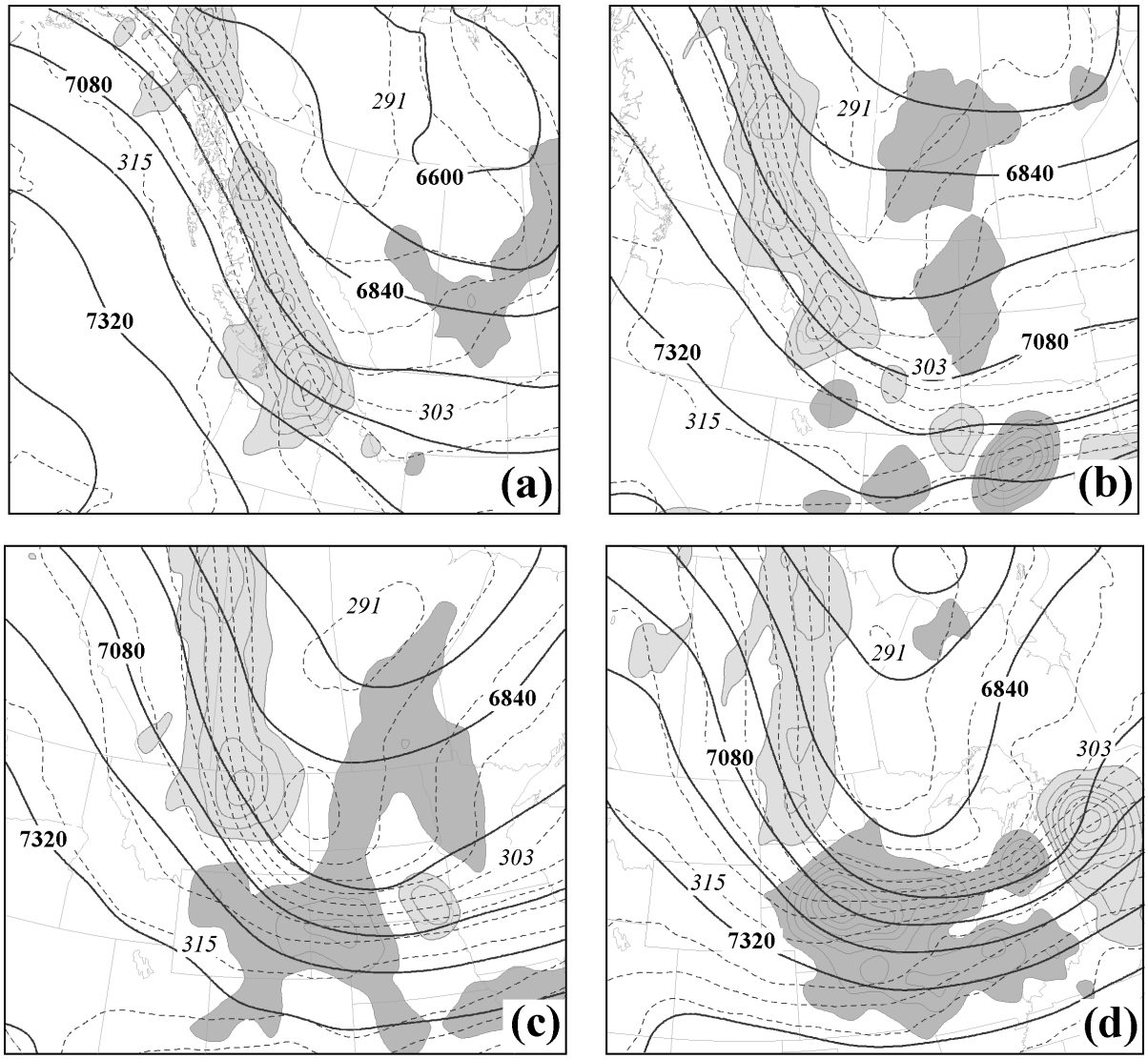

Fig. 15 (a) 400 hPa geopotential height (solid lines), isentropes (dashed lines) and geostrophic temperature advection (shading) from the Eta model analysis valid at 1200 UTC 11 November 2003. Geopotential height labeled in m and contoured every 120 m. Isentropes labeled and contoured as in Fig. 6a. Dark (light) shading represents negative (positive) geostrophic temperature advection labeled in units of K s^{-1} and contoured every –2 (2) x 10^{-4} K s^{-1} beginning at –2 (2) x 10^{-4} K s^{-1}. (b) As for Fig. 15a but from the Eta model analysis valid at 0000 UTC 12 November 2003. (c) As for Fig. 15a but from the Eta model analysis valid at 1200 UTC 12 November 2003. (d) As for Fig. 15a but from the Eta model analysis valid at 0000 UTC 13 November 2003.

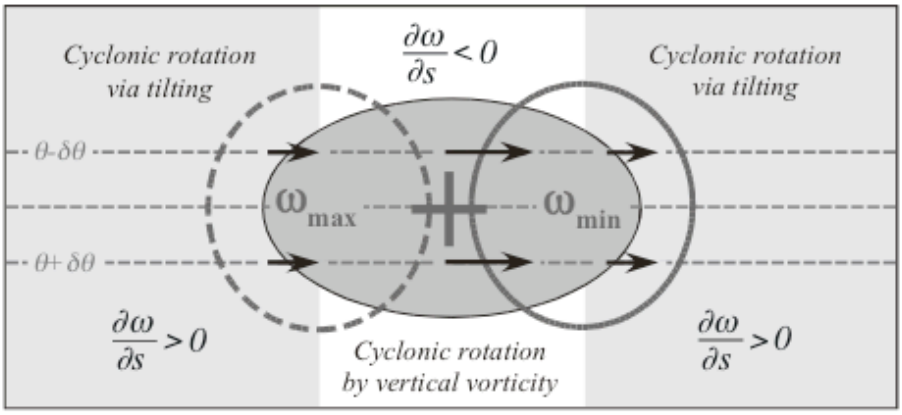

Fig. 16 Schematic illustrating the mechanisms by which positive rotational frontogenesis is induced in the vicinity of an isolated vertical vorticity maxima. Dark shaded oval represents the vertical vorticity maxima. Black arrows are the associated $\boldsymbol{Q}_s$ vectors. Thin dashed lines are isentropes. Convergence (divergence) of $\boldsymbol{Q}_s$ downshear (upshear) of the vorticity maxima is associated with ascent (descent) indicated by the thick solid (dashed) lines. Lightly shaded regions upshear and downshear of the vorticity maxima are characterized by positive rotational frontogenesis induced by along-shear tilting (i.e. $\frac{\partial \omega}{\partial s} > 0$). In the unshaded center region, $\frac{\partial \omega}{\partial s} < 0$ and positive rotational frontogenesis is forced instead by cyclonic rotation associated with the vertical vorticity maxima. See text for additional explanation.